Developing an Unmanned Aerial Remote Sensing of ET System

Final Project Report

José L. Chávez, Associate Professor, Civil and Environmental Engineering Department, Colorado State University,

Introduction

Remote sensing ET models are being used in agricultural irrigation water management. These models either rely on distributed information on surface vegetation indices (visible and near infra-red bands) or/and on surface temperature images (Gowda et al., 2008). RS of ET models perform better on certain regions, environments and surface conditions. Therefore, there is a need to assess a reliable RS of ET model for Colorado. Furthermore, a main challenge regarding RS imagery, is that the temporal resolution of multispectral satellite images is not adequate (e.g., every 16 days in the case of Landsat 8) to estimate daily crop ET. If there is cloud cover during a satellite overpasses then estimates of ET for a month will not be possible. Using airborne RS platforms may be cost-prohibited (~$5,000 per campaign/farm) and may not be available on demand (due to the nature of their commercial applications and commitments). Therefore, it is believed that with the integration of multispectral sensors in a small unmanned aircraft system (sUAS), a robust and dependable high spatial resolution ET model can be developed.

With this project it was possible to acquire and instrument a small Unmanned Aerial Vehicle (sUAV). Multispectral RS sensors were mounted on the aerial platform. Additional funds were secured from the Borland Hydrology Grant (CSU Civil and Environmental Engineering Department).

The research reported in this document used remote sensing (RS) sensors mounted on a small unmanned aerial system (sUAS). Data derived from the aerial RS platform were used to apply and evaluate a RS algorithm of crop evapotranspiration (ET) method for suitable for eastern Colorado.
The type of information that was sought to be gained included: a) suitable RS of crop ET algorithm for eastern CO; b) ability to map (monitor) ET at high spatial resolution with the UAS; and c) documentation of spatial crop water stress and ET not used.

The objectives of the research, for the 2015 crop growing season, included: use of the sUAS remote sensing data in remote sensing of crop evapotranspiration (ET) methods and adjustment of most promising method, if needed, for eastern Colorado for the crops used in the study.

Methodology

The different research locations, were RS data were collected using the UAS, include: a) turf grass plots, managed under sprinkler irrigation, near Berthoud, CO (at Northern Water, NW); b) a furrow irrigated sorghum field, near Rocky Ford, CO (CSU Arkansas Valley Research Cener, AVRC); where two large weighing lysimeters are located; and c) irrigated corn plots available at CSU Agricultural Research Development and Education Center (ARDEC), near Fort Collins, CO.

Remote Sensing data from the UAS were used in five ET algorithms: a) a two-source energy balance (TSEB) model, b) a surface aerodynamic temperature EB model (SAT), c) a crop water stress index (CWSI) model, d) a reflectance based NDVI or Normalized Difference Vegetation Index adjusted crop coefficient model, and e) a reflectance based fractional vegetation cover (fc) adjusted crop coefficient model. Resulting actual crop ET (ETa) values were evaluated with ET derived from a soil water balance (SWB) approach. For the SWB, soil water content (SWC) sensors/instrument (i.e., neutron probe, NP), and lysimetric ET data, were used along with rainfall and irrigation amounts.

A description of each RS of ET method used in this study, with the CSU UAS, can be found in Appendix A.

Description of the data acquisition location: At ARDEC, irrigation treatments range from full (100%) to limited (at crop establishment and at reproductive stages) to drought where only one irrigation was applied. Four replicas of each treatment were available at field 1070 (ARDEC). Figure (1) shows the location of the experiment and irrigation treatments at ARDEC. Irrigation was with a self-propelled linear move. Corn was grown at field 1070. Other crops included sorghum (at AVRC) and turf grass (NW).

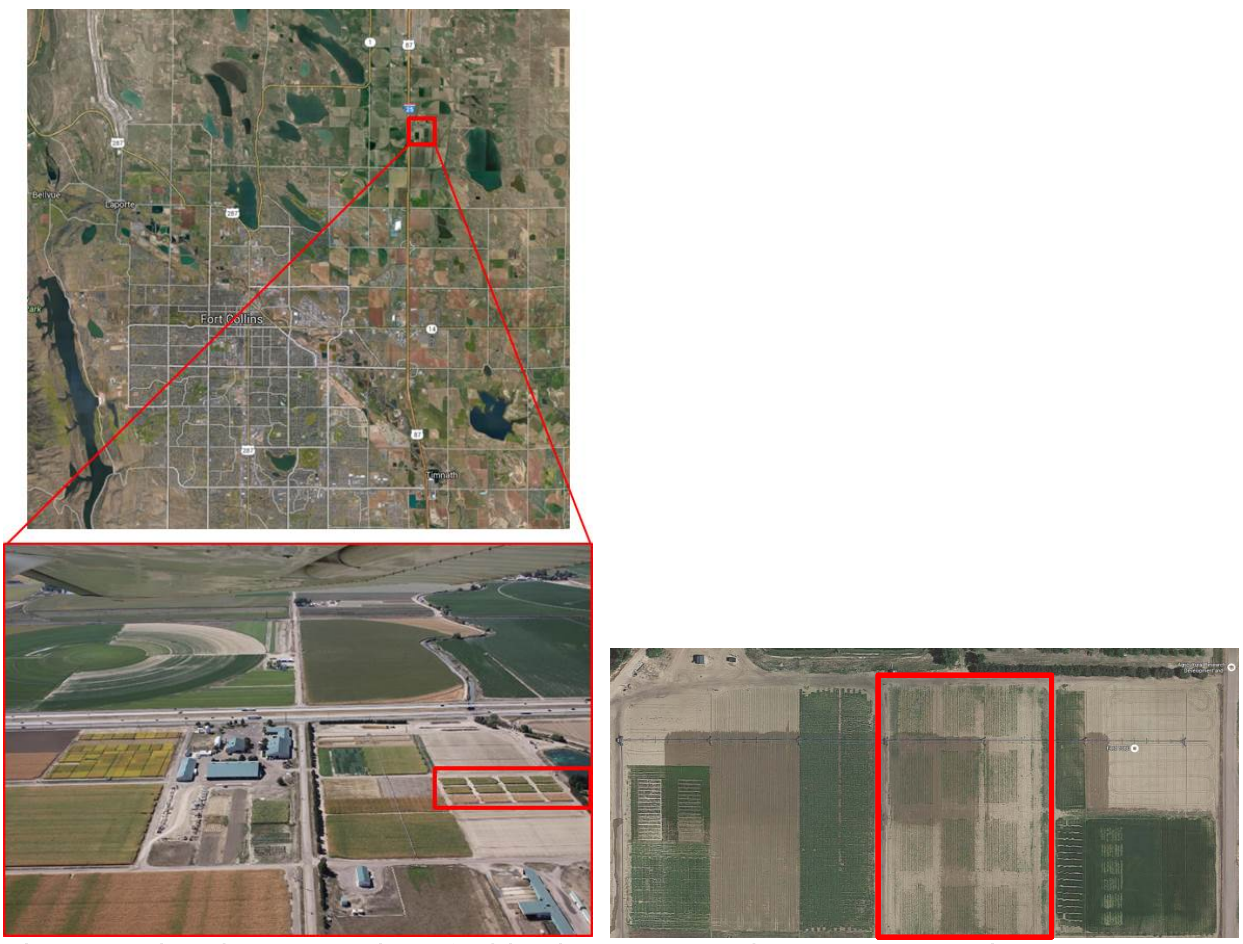

Figure 1. The pictures on the left side show CSU Agricultural Research Development and Education Center (ARDEC), near Fort Collins, CO. In this picture, field 1070 (red

rectangle) displays the three irrigation treatments and four replicas. The picture on the right side shows field 1070 being partially irrigated (linear move).

A small UAS was used to collect multispectral remote sensing data. The CSU Tempest UAS is a fixed wing commercially available UAS. The USA is operated by an Autonomous Flight Control (AFL) from launch to recovery. The CSU Tempest UAS is capable of conducting RS missions with an eleven pound payload. Besides the AFL, a manual radio frequency (RF) control is available with the system. The system technical specifications are detailed in table 1 below. The UAS is shown is Figure 2.

Table 1. CSU Tempest UAS technical specifications.

Specifications	
Wingspan	127" (251 mm)
Wing Area	1016 sq in (0.65 sq m)
Empty Weight	10 lbs (4.54 kg)
Nominal GTOW	11 lbs (5 kg)
Maximum GTOW	20 lbs (9.07 kg)
Wing Loading	20.6 oz/sq ft
Length	61.375" (1524 mm)
Airfoil	MH-32
Center of Gravity	3.5" from leading edge of the wing (89mm)
Stall Speed	20 mph
Cruise Speed	50 mph
Max Speed	100 mph
Max Range	60 mi (52.14 NM)
Radio Range	10 mi (8.69 NM)
Flight Time	1.5 HR

Figure 2. The CSU Tempest UAS mounted on a tripod for display.

The CSU Tempest UAS was initially integrated with five (5) sensors designed to collect data over the Blue, Green, Red, Near Infrared, Mid Infrared, and Thermal wavelengths of the Electromagnetic Spectrum. The sensors are controlled through the Tempest Autopilot (except the MSR5, described below, which was controlled by a separate board). Table 2 describes the specifications of the sensors while Figure 3 shows pictures of the cameras used.

Table 2. Description of sensors mounted on the CSU UAS.

CSU Tempest RS Payload			
Sensor	**Collection Priority**	**Wavelengths**	**130 m (AGL) Resolutions**
MSR5 Multispectral Scanner	Blue	450-520 nm	24.77 m
	Green	520-600 nm	
	Red	630-690 nm	
	NIR	760-900 nm	
	Thermal	1550-1750 nm	
Exergen Infrared Thermometer	Thermal	6.5-14 µm	17.61 m
FLIR Tau 2 640	Thermal	7.5-13.5 µm	11.76 cm
Tetracam ADC SNAP	NIR	520-920 nm	6.5 cm
	Red		
	Green		
Sony A6000	Visible	450-690 nm	9.5 cm

		
FLIR Tau 2 640	Tetracam ADC SNAP	Sony A6000

Figure 3. Pictures of cameras integrated into the CSU Tempest UAS.

At ARDEC field 1070 there were five (5) UAS RS campaigns. The dates were: July 15, 22, and 30, August 13, and September 10 of 2015. The CSU AVRC and NW fields were covered on September 18 and 23, respectively.

Below follows details on the flights' settings of integrated sensors:

- Flight elevation levels: 150 – 400 ft AGL (Above Ground Level)
- UAS speed: 18 m/s
- Imagery pixel resolution:

    - RED, NIR bands: 2.4 – 6.5 cm (Tetracam Snap ACD)
    - Thermal camera: 4.4 – 11.7 cm (FLIR TAU 2 640)
    - Visible: 3.5 – 9.5 cm (Sony A6000)
    - Multi-Spectral scanner: 9.3 – 24.8 m (MSR5)
    - Infra-red Thermometer: 8.8 – 17.6 m (Exergen IRT)
  - Autonomous Flights for data collection with manual control backup.
  - The imagery were geo-referenced with GPS data from reference markers installed at field 1070.

Imagery Pre-processing procedure

- **Raw Data Conversion:**
  - Multispectral – PixelWrench 2 Software convert the raw data file to the False Color (NIR, Red, Green) Digital Number (DN) .tiff formatted file.
  - Thermal – ThermalViewer Software converts the raw data file to a Radiometric or DN .tiff
- **Sensor Geometric Calibration:**
  - A6000 and FLIR Tau 2 imagery were geometrically calibrated, using ERDAS Imagine software to remove distortion from the imagery.
  - The PixelWrench 2 Software was use to perform the geometric calibration for the Tetracam ADC Snap.
- **Geo-Rectification:**
  - All of the ".tiff" formatted files were geo-rectified using ERDAS Imagine.
- **Image Mosaicking:**
  - Images were mosaicked using ERDAS Imagine to produce the Thermal, Multispectral and Visible Imagery of the target area (field).
- **Spectral Calibration:**
  - Thermal Imagery – The thermal images were further calibrated for the current conditions (removing atmospheric effects) utilizing the data from the ground based IRTs.
  - Multispectral optical imagery were calibrated for the current condition (removing atmospheric effects) utilizing the data from the ground based MSR5 multispectral scanner.
  - Calibration data was collected from both the ground and by UAS over the White, Black and Soil References.
    - White Reference – Spectralon reflectance panel (Figure 4, right)
    - Black Reference – Black Panel (Figure 4, left)
    - Soil Reference – Bare Soil

Figure 4. Black (left) and white (right) reflectance panels used for optical imagery reflectance calibration.

Once surface reflectance and temperature were obtained with the UAS then the ET algorithms detailed in Appendix A were used to map crop water used. Estimated actual ET values were compared to ET values derived from a SWB. The SWB approach followed was:

$$ET_a = (VWC_{i-1} – VWC_i) \times 1000 \times Rz + Pe + Ie \tag{1}$$

where: ET_a is actual crop evapotranspiration (mm/d), VWC is soil volumetric water content (m^3 m^{-3}) measured with a neutron probe soil moisture sensor at intervals of 0.3 m in the soil profile from 0.3 – 1.5 m of soil depth. Subscript “i” indicates a particular day of the year. Therefore, for a daily SWB, VWC would be measurements from two consecutive days. Soil water status (VWC) data were collected at eight (8) locations (NP access tubes) within the corn plots in field 1070. The 1000 factor is to convert the VWC values from m^3 m^{-3} to mm/m (mm of water per m of soil depth), Rz is the soil root zone depth, Pe (mm) is the effective precipitation or rainfall (gross amounts taken from on-site weather station), and Ie is the effective irrigation (mm). To convert from gross to effective we used a factor of 0.9.

Statistical Analysis

Comparison was made between the crop actual ET (ETa), estimated using the remote sensing algorithms, with the crop ETa derived from the soil water balance. The comparison was done using the mean bias error (MBE) and the root mean square error (RMSE) parameters, which are defined below.

The MBE is usually used to determine the average model bias or average over- or under-prediction. MBE is obtained by summing up the differences between predicted and observed values. Positive values indicate model over-estimation bias, and negative values indicate model under-estimation bias (Willmott 1982; Katiyar et al., 2010), and zero is interpreted as absence of bias and not necessarily absence of error.

$$\mathrm{MBE} = \frac{1}{n}\sum_{i}^{n}(\,M_i - O_i) \qquad (2)$$

where O is the observed (measured) value and M is the predicted or derived (remote sensing based in this case) value.

The RMSE is commonly used as an error index statistic. A smaller RMSE value indicates a smaller error spread and variance and therefore a better model performance. It measures the magnitude of the spread of errors, squaring errors before averaging them. Therefore, the RMSE gives a relatively high weight to large errors. Willmott (1982) defines RMSE as:

$$\mathrm{RMSE} = \sqrt{\frac{1}{n}\sum_{i}^{n}(\,M_i - O_i)^2} \qquad (3)$$

Results

During the first three flights/dates the thermal camera system did not store data and the shortwave optical camera was intermittent. The cameras' interface and autopilot program were modified to fix the problem. Thus, in this study, for the ARDEC field 1070 only was possible to have complete data sets (optical and thermal) for August 13th and September 10th. On July 22nd and 30th only optical (visible and near infra-red bands) data were obtained. For those days when only the optical imagery were available then only the reflectance based crop coefficients methods (based on NDVI and Fc), to obtain ET_a, were applied.

The verification of the thermal imagery surface temperature values performed with ground based IRTs and a FLIR handheld camera (thermography, Figure 5) indicated the thermal imagery surface temperature RMSE was around 0.5 °C. This is considered a very good result and the thermal imagery (data) were determined to be accurate.

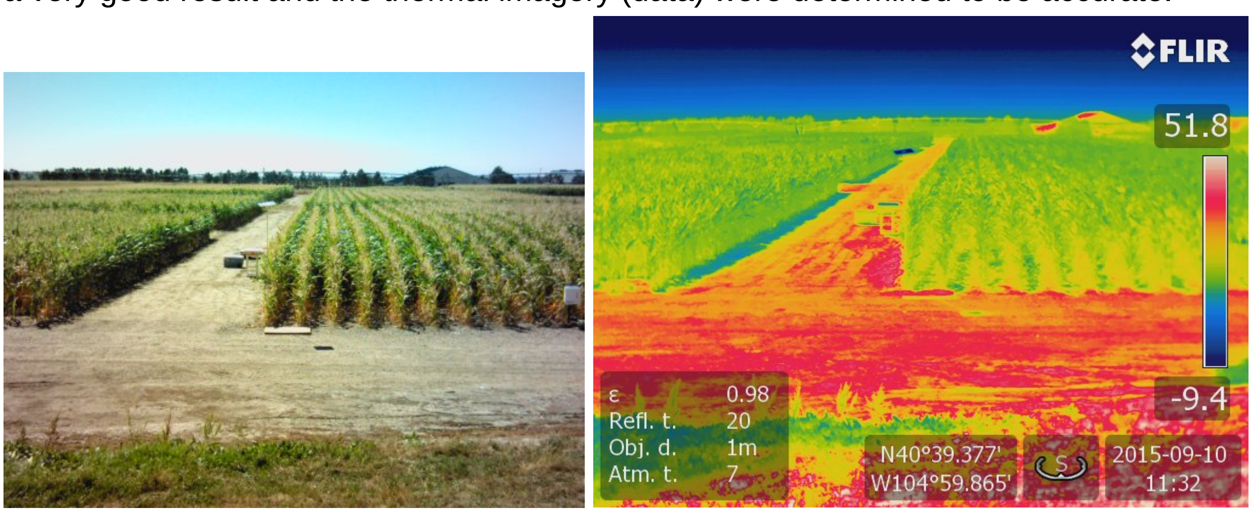

Figure 5. Handheld FLIR 650C Thermal camera captured RGB picture (left) and thermal image (°C) of field 1070 (CSU ARDEC) on 10 September 2015. Different locations were sample at plots/treatments and on soil, water, and surrounding fields as well for the evaluation of the UAS thermal imagery.

A sample of the data collected with the UAS multispectral RS system is displayed in Figures 6 and 7 below.

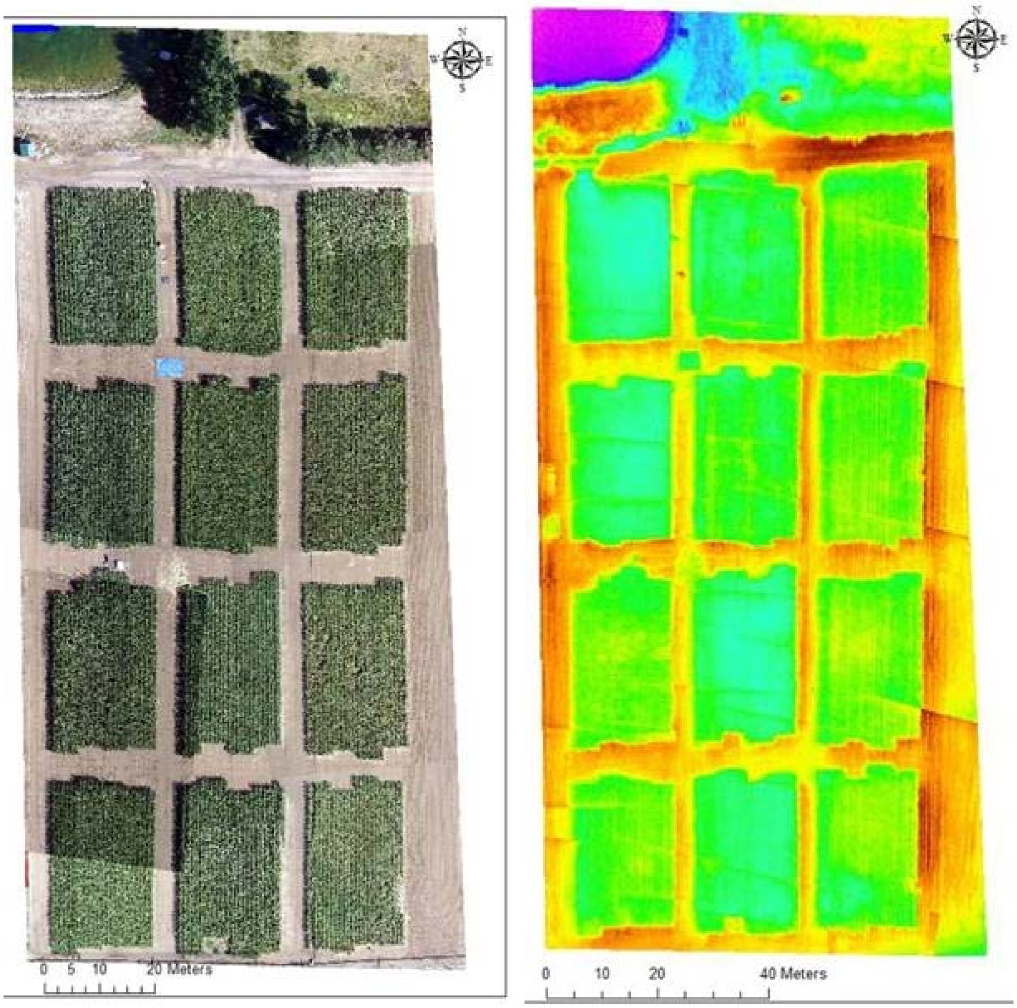

Figure 6. A6000 RGB digital camera picture (left) and FLIR Tau 2 thermal image acquired on 13 August 2015 at 11:30 a.m. MDT. The surface temperature obtained from the thermal imagery indicated that the ranged from 14 to 36 °C. The A6000 camera acquired regular RGB pictures at a spatial resolution of 9.4 cm per pixel. The thermal camera spatial resolution was 11.7 cm per pixel for a flight altitude of 121 m AGL.

The individual shortwave bands, captured with the Tetracam, were combined (stack, NIR first, followed by Red and by Green bands, in that order) after rectification and calibration to produce a false color 3-band imagery (Figure 7). In the 3-band image (right), the green color of leaves are shown as red and it is evident from the reflectance image that the four plots on the east side of field 1070 had less red color which meant less biomass or leaves. This was expected for the drought irrigation treatment located on that side of the field. Therefore, the Tetracam camera was able to capture appropriately the reflectance of the different irrigation treatments.

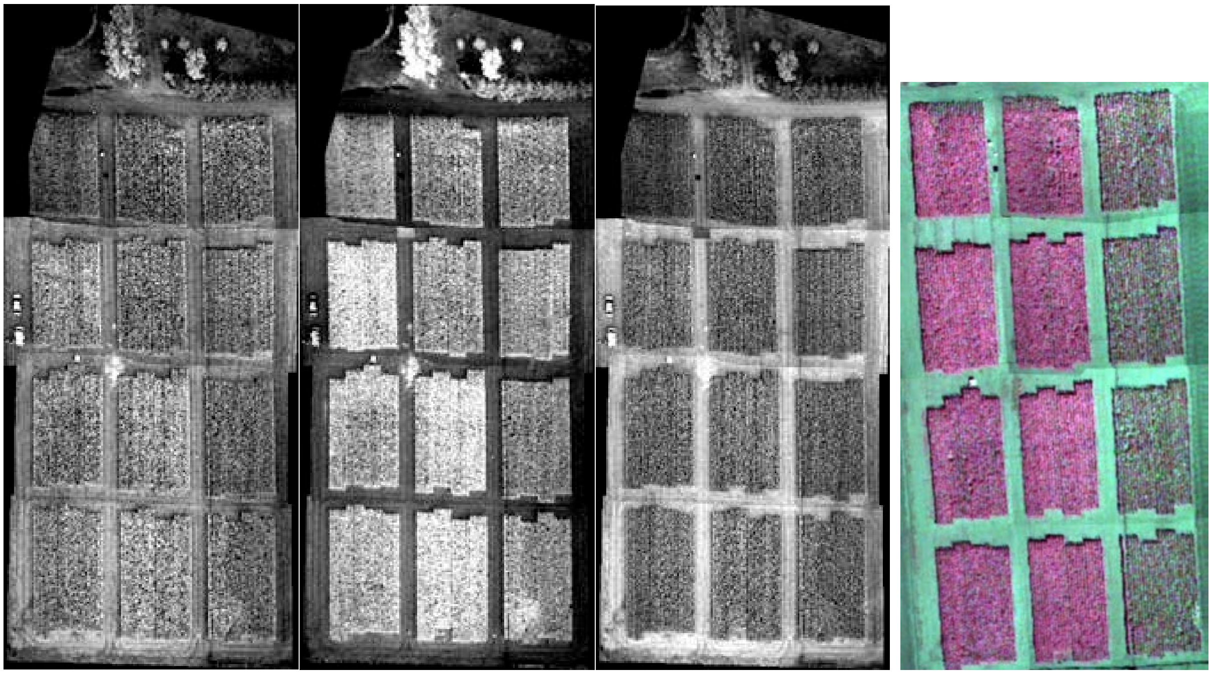

Figure 7. From left to right: Green, NIR, Red bands, and a resulting 3-band stack false color image. Data acquired on 13 Aug 2015 over field 1070 at ARDEC.

After obtaining field surface reflectance and temperature imagery and applying the different RS of ET algorithms, ET_a values, from the UAS, were compared to similar values derived from the NP SWB. Figure 8 plots VWC for one of the NP access tubes.

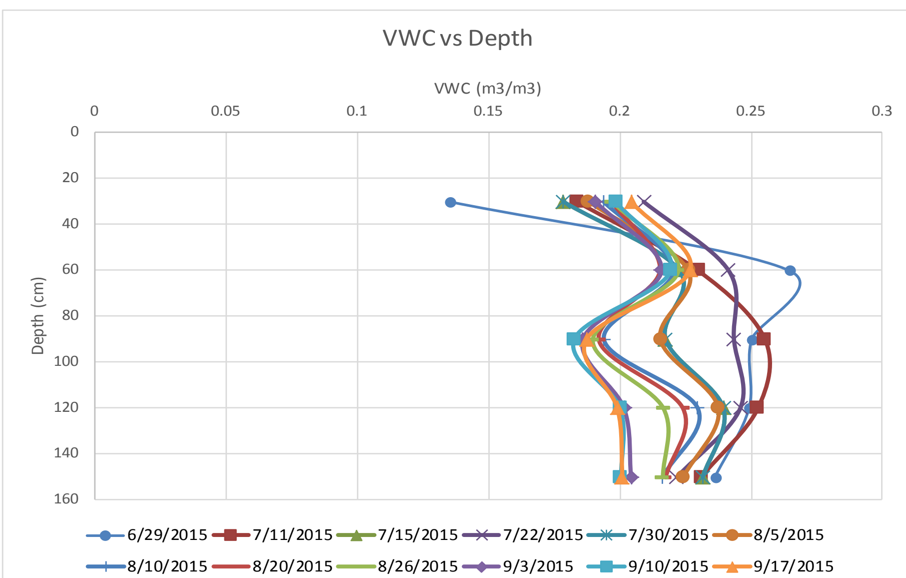

Figure 8. Soil volumetric water content (m^3 m^{-3}), measured with a neutron probe at different soil depths on different date throughout the corn growing season, at a fully irrigated treatment in field 1070 ARDEC.

From the NP seasonal data it was determined that the corn was extracting water from the soil profile from all depths (layers) where data were collected (up to 1.5 m). This result is an indication that the fix irrigation schedule (once a week) and amount (of 1 inch or 25.4 mm) for field 1070 fully irrigated plots did not return the soil water content to field capacity throughout the crop root zone. As the crop season progressed, the corn extracted more water from deeper soil layers. Therefore, it was expected that even the "fully" irrigated plots would have suffered from some water stress.

To verify this finding another soil water balance was performed. This SWB was based on estimates of crop water use (ETc) for non-stressed corn using weather data from the in-situ COAGMET weather station and the irrigation and rainfall data. The methodology indicated in Andales and Chávez (2011) and Andales et al. (2011) were followed to apply the new SWB. Figure 9 shows the resulting SWB.

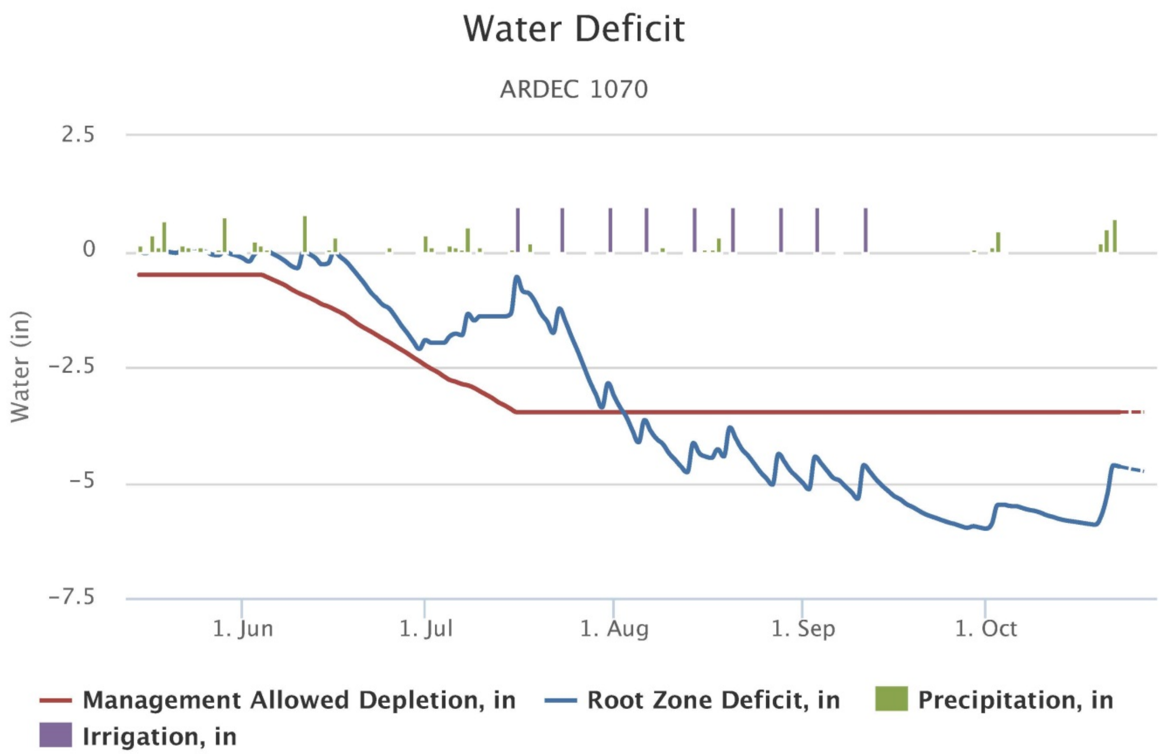

Figure 9. Soil water depletion at ARDEC field 1070 throughout the 2015 corn growing season based on weather station data derived ET in soil water balance.

From Figure 9 plot, it is evident that after August 1st the soil water content in the crop root zone was not sufficient to sustain a full ET rate. The plant roots had extracted water from the soil beyond the set soil management (or allowed) depletion, potentially causing water stress and an ET rate less than "potential" or optimal. Thus, this result confirms the findings of seasonal soil water depletion (extraction) found with the neutron probe data.

Estimated values of actual corn ET (for ARDEC) using the different (5) RS of ET algorithms were plotted versus ET_a values derived from the NP data and the SWB

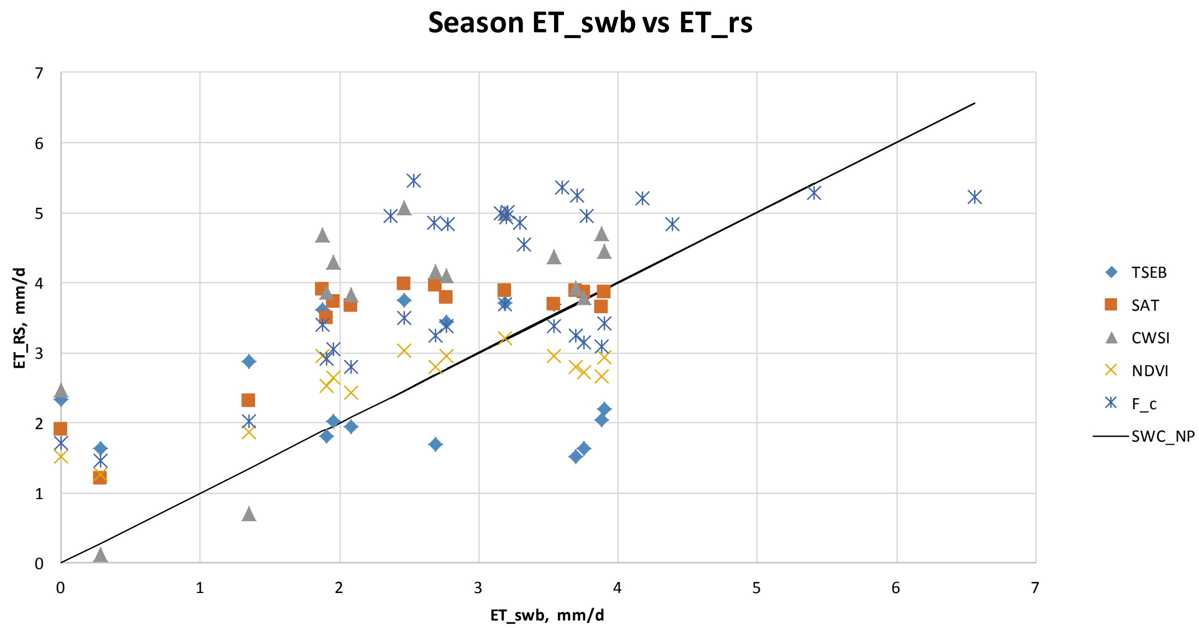

Figure 10. Comparison of corn actual ET estimated with a RS algorithm and corresponding values of ET derived from a SWB and measured soil water.

method. Figure 10 shows the scatter plot where the x-axis is the ET from the SWB (ET_swb) while the y-axis is the ET from one of the RS methods (i.e., TSEB for the Two-Source-Model, SAT for the surface aerodynamic temperature energy balance model, CWSI for the Crop Water Stress Index method, NDVI for the reflectance based crop coefficient based on NDVI, and F_c for the reflectance based crop coefficient based on fractional vegetation cover). The graph also shows a 1:1 line (black line), denoted SWC_NP, to visually observe how close estimated ET values were to "measured" values. This is, the closer the points to the 1:1 line the more accurate the method in estimating actual crop ET.

Maps of ET_a (mm/d) for the different ET methods and locations can be found in Appendix B.

From Figure 10 visual observation one can see that both methods based on adjusting the crop coefficient (i.e., using NDVI and fc from RS) had points closer to the 1:1 line. Thus, the NDVI and F_c ET points seem to estimate corn ET more accurately than the other RS of ET methods.

The statistical analysis is shown in Table 3 where the Kc_NDVI (or NDVI) method resulted with the lowest ET_a (mm/d) MBE and RMSE values, followed by the Kc_fc (or Fc) method. The third best performing RS of ET algorithm was the SAT method based on the land surface energy balance which showed acceptable errors. One possible cause of the somewhat over estimation of ET_a by this SAT method may be the fact that wind speed data were obtained from the COAGMET weather station when the method calls for measuring wind speed on-site; ie., about 2 m above the corn canopy. The

CWSI method also over estimated actual corn ET values. Perhaps this result may have been caused because air temperature and relative humidity were obtained from the COAGMET weather station and not measured on-site as the method prescribes. The worst performing method was the TSM (TSEB). This method is very data and processing intense and there are many instances in which errors can be committed.

Table 3. ET_a (mm/d) mean bias error (MBE) and root mean square error (RMSE) results.

	TSEB	SAT	CWSI	NDVI	Fc
MBE	2.50	0.97	1.26	0.28	0.96
RMSE	2.63	1.21	1.63	1.07	1.38
n	16	16	16	24	32

Note: n is the sample size.

The statistical analysis was further broken down, for the ARDEC data, into RS days/campaigns to observe in more detail the performance of the RS of ET methods under different conditions. Tables 4, 5 and 6, below, show the actual ET errors for July 22nd and 30th, August 13th, September 11th, respectively.

For the vegetative growth stage of corn at ARDEC, the reflectance based crop coefficient adjusted with NDVI resulted with less error than the crop coefficient adjusted with fractional vegetation cover (Fc), as shown in Table 4.

Table 4. Actual corn ET for July UAS flights for the reflectance-based crop coefficient method (i.e., NDVI and Fc).

	22-Jul	30-Jul	
Method	Fc	NDVI	Fc
MBE, mm/d	1.64	1.46	1.81
RMSE, mm/d	1.30	0.82	1.05
MBE, %	21.7	7.4	16.2
RMSE, %	23.9	18.0	22.3

By mid August the corn had reached the reproductive growth stage and the fully irrigated treatment had reached full cover. Under these conditions, the Fc method performed very well resulting with the lowest MBE±RMSE of 0.13±0.75 mm/d. This method performance was closely followed by the NDVI crop coefficient (Kc) method and then by the SAT energy balance method with acceptable ET_a estimation errors. The other two methods, the TSM (TSEB) and the CWSI method had errors that are deemed large for purposes of improving irrigation water management.

Table 5. Actual corn ET for all methods for the August 13th UAS flight.

			13-Aug		
Method	TSEB	SAT	CWSI	NDVI	Fc
MBE, mm/d	-1.12	0.79	1.14	-0.29	0.13
RMSE, mm/d	1.43	1.12	1.40	0.81	0.75
MBE, %	-16.9	11.9	17.3	-4.4	2.0
RMSE, %	21.7	16.9	21.1	12.3	11.3

For the UAS RS flight of 10 Sept 2015, a similar performance of RS of ET methods was obtained. This is, the NDVI based Kc and the Fc Kc methods performed better; followed by the SAT energy balance method. Larger errors in estimating ET_a were found for the CWSI method.

Table 6. Actual corn ET for all methods for the September 10th UAS flight.

			11-Sep		
Method	TSEB	SAT	CWSI	NDVI	Fc
MBE, mm/d	1.20	1.15	1.38	0.54	0.89
RMSE, mm/d	1.37	1.30	1.83	0.82	1.05
MBE, %	13.8	13.3	16.0	6.2	10.3
RMSE, %	15.8	15.0	21.2	9.5	12.2

Results of ET_a, from the UAS flight on September 18th over a sorghum field at the CSU AVRC facility near Rocky Ford, CO, were as followed: TSM = 5.6 mm/d, SAT = 4.2 mm/d, and Fc (or Kc, Kcr) = 4.0 mm/d. While the lysimeter measured sorghum ET_a was 4.6 mm/d. The alfalfa reference ET (ETr) was 6.6 mm/d on that day and the expected non-water-stress sorghum ET (ETc) was about 5.2 mm/d (as per tabulated crop coefficients). Thus, the SAT method produced an ET_a rate closer to the measured by the lysimeter at Rocky Ford. Most probably this better performance of the SAT method over a sorghum field has to do with weather data collected in-situ (mainly wind speed) and the fact that the field was large and therefore ensuring sufficient fetch (footprint) for the valid application of the method. The reflectance based coefficient (Fc) performed relatively well. However, the TSM overestimated ET by 1.0 mm/d.

Results of ET_a, from the UAS flight on September 23rd over turf grass at NW near Berthoud, CO, were as followed: TSM = 2.5 mm/d, CWSI = 1.3 mm/d, SAT = 3.4 mm/d, NDVI Kc = 2.6 mm/d, and Fc Kc = 2.9 mm/d. While the soil moisture sensor derived ET_a was 2.3 mm/d. For the grass vegetation the NDVI Kc RS of ET method resulted with the more accurate estimation of ET_a followed by the TSM method and by the Fc Kc method. Both the CWSI and SAT methods did not performed well in this case.

Conclusions

A fix-wing small unmanned aerial system (sUAS) was equipped with multispectral remote sensing sensors. Some issues were encountered regarding the integration of the sensors with the on-board autonomous control system that prevented the acquisition of a large number of images (flight campaigns) during the crops growing season. However, the CSU Tempest UAS is capable of acquiring optical and thermal data (images) for input into algorithms to estimate crop water use, for instance.

Five different remote sensing of ET algorithms were applied using the UAS data. Evaluation of the actual ET values obtained revealed that the reflectance based crop coefficient methods (i.e., NDVI and vegetation fractional cover) performed better (more accurate) than the full land surface energy balance methods (i.e., TSM and SAT), being the least accurate the CWSI method.

For corn, the SAT performed relatively well and it seems that if weather data are collected in-situ the method has potential to perform better.

For sorghum, the SAT and the vegetation fractional cover adjusted crop coefficient methods performed better. While for turf grass, the TSM and the reflectance based crop coefficient (based on NDVI) performed better.

From these results, it can be concluded that the CSU Tempest UAS has the potential to estimate crop water use with similar accuracy and errors as methods used with satellite and manned airborne platforms. Regarding the remote sensing of ET, the methods based on adjusting crop coefficients with reflectance images seemed to performed best for all vegetation types used in this study; followed by the SAT method. However, the application of one given method under different surface and environmental conditions may produce different results. This is, it seems that a give RS of ET method tends to perform better under certain conditions (e.g., field size, crop growth stage and biomass amount or LAI, weather conditions, soil moisture conditions, etc.). Further research is needed, using UASs, to incorporate a large set of data over a range of crop/vegetation and environmental conditions to establish (assess and calibrate) the best combination (hybrid) of ET methods for crops grown in Colorado.

Acknowledgment

Financial support was received from Colorado Water Conservation Board (CWCB) through Colorado Water Institute (CWI). Likewise this study was possible thanks to support received from Colorado State University (CSU), Civil and Environmental Engineering, Borland fund (support for studies in hydrology). The experiment carried out at ARDEC field 1070 was mainly supported by a grant from the USDA Natural Resources Conservation Service (NRCS) Conservation Innovation Grants (CIG) program. From the CIG project we thank Drs. Neil Hansen, Francesca Cotrufo and Allan Andales. The participation of the following CSU students is greatly appreciated: Jeff Hathaway, Kyle Page, David Andales, Amandeep Vashisht, Sumit Gautam, Emily Kullberg, Erika Foster and Abhinaya Subedi. Technical support for the UAS was received from UASUSA and BlackSwift. Finally we are thankful for the collaboration received from Mark Collins and Christopher Fryrear from CSU ARDEC.

REFERENCES

Andales, A.A., and J.L. Chávez. 2011. ET-based Irrigation Scheduling. In Proceedings of the 23rd Annual Central Plains Irrigation Conference, Burlington, Colorado, Feb. 22-23, 2011, Central Plains Irrigation Assoc., Colby, Kansas.

Andales, A., Chávez, J.L., and Bauder, T.A. 2011. Irrigation Scheduling: The Water Balance Approach. Colorado State University Extension. Factsheet No. 4.707. Published on-line, July 2011.

ASCE-EWRI. 2005. The ASCE Standardized Reference evapotranspiration Equation, Task Committee on Standardization of Reference Evapotranspiration, Environment and Water Resources Institute of the ASCE, 2005; pp. 200.

Brest, C.L., and S.N. Goward. 1987. Driving surface albedo measurements from narrow band satellite data. International Journal of Remote Sensing, 8:351-367.

Brutsaert, W., 1975. On a drivable formula for long-wave radiation from clear skies. Water Resour. Res. 11, 742-744.

Campbell, G.S. 1986. Extinction coefficients for radiation in plant canopies calculated using an ellipsoidal inclination angle distribution. Agricultural and Forest Meteorology, 36:317-321.

Campbell, G.S., and J.M. Norman. 1998. An introduction to environmental biophysics. 2nd Ed., Springer Verlag, New York.

Chávez, J.L.; Neale, C.M.U.; Hipps, L.E.; Prueger, J.H.; Kustas, W.P. 2005. Comparing aircraft-based remotely sensed energy balance fluxes with eddy covariance tower data using heat flux source area functions. Journal of Hydrometeorology, 2005, 6, 923-940.

Chávez, J.L.; Neale, C.M.U.; Prueger, J.H.; Kustas, W.P. 2008. Daily evapotranspiration estimates from extrapolating instantaneous airborne remote sensing ET values. Journal of Irrigation Science, 2008, 27(1), 67-81.

Chávez J.L, Gowda P.H., Howell T.A., Neale C.M.U., and Copeland K.S. 2009. Estimating hourly crop ET using a two-source energy balance model and multispectral airborne imagery. Irrigation Science Journal 38:79-91.

Foken T (2006) 50 Years of the Monin–Obukhov similarity theory.Boundary-Layer Meteorol 119(3):431–447.

Goudriaan, J. 1977. Crop micrometeorology: A simulation study. Center for Agriculture Publication Documentation, Wageningen, The Netherlands.

Gowda, PH., J.L. Chávez, P.D. Colaizzi, S.R. Evett, T.A. Howell, and J.A. Tolk. 2008. ET mapping for agricultural water management: present status and challenges. Irrigation Science J. 26(3): 223--237.

Hoffman, G.J., R.G. Evans, M.E. Jensen, D.L. Martin, and R.L. Elliott. 2007. Design and Operation of Farm Irrigation Systems. 2nd Ed., ASABE, St. Joseph, MI, 1040 pp. ISBN: 1-892769-64-6.

Idso, S.B.; Jackson, R.D.; Pinter Jr., P.J.; Reginato, R.J.; Hatfield, J.L. 1981. Normalizing the stress-degree-day parameter for environmental variability. Agricultural Meteorology 1981, 24(1), 45-55.

Idso, S.B. 1982. Non-water-stressed baselines: A key to measuring and interpreting plant water stress. Agricultural Meteorology 1982, 27(1-2), 59-70.

Johnson L.F. and T.J. Trout. 2012. Satellite NDVI Assisted Monitoring of Vegetable Crop Evapotranspiration in California’s San Joaquin Valley. Remote Sens. 2012, 4, 439-455; doi:10.3390/rs4020439.

Katiyar AK, Kumar A, Kumar Pandey C, Das b (2010) A comparative study of monthly mean daily clear sky radiation over India. *International Journal of Energy and Environment*. 1(1): 177-182.

Kustas, W.P., and J.M. Norman. 2000. A two-source energy balance approach using directional radiometric temperature observations for sparse canopy covered surfaces. Agronomy Journal, 92:847-854.

Liu, S., D. Mao, and L. Lu. 2006. Measurement and estimation of the aerodynamic resistance. Hydrol. Earth Syst. Sci. Discuss., 3:681-705.

Monteith, J.L. 1973. Principles of environmental biology. Edward Arnold Press, Kent, U.K.

Monteith and Unsworth, 1990. Principles of Environmental Physics. 2nd Edition, Edward Arnold Press, 1990. Chapter 6, “Momentum Transfer”, page 97.

Neale C.M.U., W.C. Bausch, amd D.F. Heerman. 1989. Development of reflectance-based crop coefficients for corn. Trans. ASAE, 32 (1989), pp. 1891–1899.

Norman, J.M., and P.G. Jarvis. 1974. Photosynthesis in Sitka Spruce (Picea Sitchensis (Bong.) Carr.) III. Measurements of canopy structure and interception of radiation. Journal of Applied Ecology, 12:839-878.

Norman JM, Kustas WP, Humes KS (1995) A two-source approach for estimating soil and vegetation energy fluxes form observations of directional radiometric surface temperature. Agric Forest Meteorol 77:263–293.

Post, D.F., A. Fimbres, A.D. Matthias, E.E. Sano, L. Accioly, A.K. Batchily, and L.G. Ferreira. 2000. Predicting soil albedo from soil color and spectral reflectance data. Soil Science Society Am. J., 64:1027-1034.

Priestley CHB, Taylor RJ (1972) On the assessment of surface heat flux and evaporation using large-scale parameters. Mon Weather Rev 100:81–92.

Spokas, K., and F. Forcella. 2006. Estimating hourly incoming solar radiation from limited meteorological data. Weed Science, 54:182-189.

Trout, T.J, and L.F. Johnson. 2007. Estimating crop water use from remotely sensed NDVI, crop models, and reference ET. The Role of Irrigation and Drainage in a Sustainable Future: Proceedings of the USCID Fourth International Conference on Irrigation and Drainage, Sacramento, CA, 3-6 October 2007. Ed A.J. Clemmens, and S.S. Anderson. 275-285.

Wilmott CJ (1982) Some comments on the evaluation of model performance. Bulleting American of Meteorological Society, 63 (11): 1309-1313.

APPENDICES

APPENDIX A
ET ALGORITHMS DESCRIPTION

Crop Water Stress Index (CWSI)

The CWSI method relies on the temperature difference (dT, ºC) between the vegetation canopy and the air (T_c – T_a), and on minimum and maximum differences in these "T_c – T_a" temperatures, as indicated in Equation A1. Air temperature measured at a height of 2.0 – 3.0 m above the ground and in the crop field.

$$CWSI = (dT - dT_{min})/(dT_{max} - dT_{min}) \quad (A1)$$

where: subscripts "min" and "max" are the minimum and maximum dT (or $T_c - T_a$), respectively. These dT boundaries can be estimated following the methodology developed by Idso et al. (1981). The dT_{min} and air water vapor pressure deficit (VPD, kPa) have a linear relationship for a fully irrigated (no water stress) crop under a given environmental condition. The dT_{max} has a linear relationship with the so called water vapor pressure gradient (VPG), when the crop is experiencing maximum water stress (dry soil to a soil water tension of about 15 bars):

$$dT_{min} = a\,(VPD) + b \quad (A2)$$

$$dT_{max} = a\,(VPG) + b \quad (A3)$$

where: the "a" and "b" coefficients are the slope and the intercept of the linear relationship between dT_{min} and VPD. The VPG is estimated as the difference between saturated air vapor pressure at air temperature and saturated air vapor pressure at air temperature plus the coefficient "b." The value of dT_{max} has also been found to be relatively constant around 4 to 5 ºC for corn fields.

The minimum dT occurs when the vegetation is not experiencing water stress. Under this condition the crop has sufficient water available in the soil root zone and the transpiration process is only limited by weather conditions. Appropriate coefficients for dT_{min}, for several crops, can be found in Idso et al. (1982). For this study, coefficients "a" and "b" were developed from in-situ field data (i.e., air temperature, vapor pressure, canopy temperature) collected one to two days after irrigation events (no water stress conditions) after corn had reach effective full cover. A linear regression was performed between dT_{min} and VPD (VPD calculation explained below). The resulting coefficients were slope "***a = -1.99***" and intercept "***b = 3.04***". These coefficients were very close to those found by Idso (1981) for corn in Arizona; which were "a = -1.97" and "b = 3.11".

In the case of dT_{max}, it occurs when the vegetation is not transpiring because the soil is very dry (soil water tension of about 15 bars) and the plant can't exert so much tension (negative pressure) to remove any more water from the soil.

To compute the vapor pressure deficit one needs readings of air temperature (T_a, ºC) and relative humidity (RH, %) obtained just above the canopy (i.e., in field or in-situ measurements); preferentially from the middle of the field. In the case of our application of the CWSI method, RH and T_a were obtained from an in-situ weather station connected to the COAGMET network. The weather station name was CSU-ARDEC (ftc03). Canopy temperature was measured with the FLIR Tau 2 thermal camera.

Vapor Pressure Deficit (VPD) Calculation

Vapor pressure deficit (VPD, in units of kilo-Pascals, kPa) was computed as follows:

$$VPD = e_s - e_a \quad (A4)$$

where, "e_s" is saturation vapor pressure (kPa) and "e_a" is actual vapor pressure (kPa), both computed as show below (where T_a is air temperature in ºC).

$$e_s = 0.6108 \times \exp\left(\frac{17.27 \times T_a}{237.3 + T_a}\right) \tag{A5}$$

$$e_a = (RH/100) \times e_s \tag{A6}$$

where, RH is relative humidity in percent (%).

Vapor Pressure Gradient (VPG) Calculation

The VPG is the difference between saturated air vapor pressure at air temperature and saturated air vapor pressure at air temperature plus the coefficient "b." Thus:

$$VPG = \left[0.6108 \times \exp\left(\frac{17.27 \times T_a}{237.3 + T_a}\right)\right] - \left[0.6108 \times \exp\left(\frac{17.27 \times (T_a + b)}{237.3 + (T_a + b)}\right)\right] \tag{A7}$$

Once the CWSI was computed the next step was to convert it to actual ET (ET_a). This computation employs the stress index and the so called potential (no stress) crop (corn in our case) ET rate. Potential corn ET values were calculated by multiplying alfalfa reference ET (ET_r) by the sum of tabulated basal corn crop coefficients (K_{cb}) and surface evaporation coefficients (K_e), Hoffman et al. (2007). Daily ET_r values were computed using weather data from COAGMET, using the standardized ASCE alfalfa reference Penman-Monteith equation (ASCE-EWRI, 2005).

Surface Aerodynamic Temperature Model (SAT)

The surface aerodynamic temperature method (SAT) was used to compute ETa values. This SAT method is a calibrated surface energy balance (EB) algorithm (Chávez et al., 2005).

Estimated corn actual water use (ET_a), from the Apogee oblique IRT-based CWSI method, was evaluated using actual ET values derived from a surface energy balance algorithm (Chávez et al., 2005). For this surface energy balance algorithm a surface bulk aerodynamic resistance model was used to obtain sensible heat flux (H).

$$H = \rho_a Cp_a (T_{aero} - T_a)/r_{ah} \tag{A8}$$

where ρ_a is humid air density (kg m^{-3}), Cp_a is specific heat of dry air (1005 J kg^{-1} K^{-1}), T_a

is average air temperature (K), T_{aero} is average surface aerodynamic temperature (K). T_{aero} (in ºC) can be expressed as (Chávez, 2005):

$$T_{aero}=0.534\,T_s+0.39\,T_a+0.224\,LAI-0.192\,U+1.67 \quad \text{(A9)}$$

where T_s is the surface radiometric temperature (°C) obtained using the FLIR Tau2 thermal camera mounted on the UAS, T_a is air temperature (°C), LAI is the leaf area index ($m^2\ m^{-2}$) derived from the TETRACAM camera mounted on the UAS, U is the horizontal wind speed ($m\ s^{-1}$). Air temperature and wind speed were collected near the field at the COAGMET weather station CSU-ARDEC. Crop height was measured periodically through the growing season. LAI was estimated using surface reflectance data acquired with the TETRACAM:

$$LAI=(4\,OSAVI-0.8)\times(1+4.73E\text{-}6\,EXP[15.64\,OSAVI]) \quad \text{(A10)}$$

where OSAVI is the optimized soil adjusted vegetation index. Sensible heat flux was corrected for atmospheric stability conditions using an iterating method as described in Chávez et al. (2005).

Net radiation was calculated as:

$$R_n=(1-\alpha)R_s+\varepsilon_a\sigma T_a^4-\varepsilon_s\sigma T_s^4 \quad \text{(A11)}$$

where R_n is net radiation ($W\ m^{-2}$), α is surface albedo, R_s is incoming shortwave radiation ($W\ m^{-2}$), σ is the Stefan-Boltzmann constant (5.67E-08 $W\ m^{-2}\ K^{-4}$), ε is emissivity, and T is temperature (K), with subscripts "a" and "s" for both air and surface, respectively.

Soil heat flux was calculated as Chávez et al. (2005):

$$G=[([0.3324+(-0.024\,LAI)]\times\{0.8155+[-0.3032\ln(LAI)]\})Rn] \quad \text{(A12)}$$

where G soil heat flux in units of $W\ m^{-2}$. Latent heat flux could then be calculated from the energy balance equation:

$$LE=R_n-G-H \quad \text{(A13)}$$

where, LE is latent heat flux ($W\ m^{-2}$). Hourly ET can be calculated using LE as:

$$ET_i=3600\,LE_i/(\lambda_v\,\rho_w) \quad \text{(A14)}$$

where, ET_i is the hourly crop actual ET (mm hr^{-1}), ρ_w is the density of water (taken as 1000 kg m^{-3}), and λ_v is the latent heat of vaporization (J kg^{-1}) equal to ((2.501 – 0.00236 Ta) x 10^6), where Ta is in ºC. Daily ET can then be calculated, (Chávez et al., 2008), from hourly ET as:

$$ET_d = \left[\frac{ET_i}{(ET_r)_i}\right] \times (ET_r)_d \tag{A15}$$

where, ET_d is crop ET daily (mm d^{-1}), $(ET_r)_i$ is the alfalfa reference hourly ET (mm hr^{-1}), and $(ET_r)_d$ is the daily alfalfa reference ET rate (mm day^{-1}).

Two-Source-Model (TSM)

The TSM algorithm solves the land surface energy balance equation (A13) for LE after finding separately the canopy net radiation R_n and sensible heat flux H and the soil R_n, soil heat flux G and H components, i.e. the TSM partitions each of the surface energy balance components into fluxes generated from the vegetation canopy (first source) and the bare soil/background soil (second source).

H is estimated by adding the soil sensible heat flux (H_{so}) that occurs between the soil surface and a point above the canopy (Z_h), where air temperature (T_a) is measured, with the canopy sensible heat flux (H_c) generated between the vegetation canopy and a parcel of air at Z_h, assuming a parallel resistance network.

The TSM is based on the so called “ensemble or composite” temperature, which is the combination of vegetation and background soil in the field of view (and pixels) of the thermal camera used, defined by equation A16 as described below.

$$T_{sfc} = [f_c\ (T_c)^4 + (1 - f_c)\ (T_{so})^4]^{1/4} \tag{A16}$$

where, T_c is canopy temperature (K), T_{so} is soil temperature (K), r_{so} is the resistance to heat flow above the soil (s m^{-1}), r_{ah} is aerodynamic resistance (s m^{-1}) to heat transfer, U_s is horizontal wind speed (m s^{-1}) just above the soil surface, ρ_a is air density (kg m^{-3}), and Cp_a is specific heat of dry air (1,004 J kg^{-1} K^{-1}). T_c and T_{so} are estimated using Eq. (A16) for a Nadir looking thermal infrared sensor/camera. The temperature measured with the UAS thermal camera was denoted T_{sfc} and is the so-called “ensemble (or composite) surface radiometric temperature,” and f_c is the fractional vegetation cover, in Eq. A16 (function of LAI).

Below is the description of some steps followed to apply the TSM in this study. To find more details in the methodology used the reader is referred to the article published by Chávez et al. (2009) “Estimating hourly crop ET using a two-source energy balance model and multispectral airborne imagery“ and Norman et al. (1995) “A two-source approach for estimating soil and vegetation energy fluxes form observations of directional radiometric surface temperature.”

First, to obtain H, an initial estimation of H_c, applying Priestly and Taylor (1972) model, is performed. Subsequently, the H_c value is used to derive an initial T_c value by inverting the H_c eq. assuming a neutral atmospheric stability condition. Next, the T_{sfc} eq. is solved for T_{so} and updated values of H_c and H_{so} are computed correcting r_{ah} for atmospheric stability using the Monin-Obukhov atmospheric stability length scale (similarity theory, Foken, 2006).

T_c and T_{so} are verified by testing the estimated LE for the soil for a negative value, in which case temperatures are not correct, and the soil is assumed to have a dry surface. Thus, a new iteration cycle is needed, in which LE is set to zero for the soil component and H_{so} is re-calculated (Hso = (Rn – G)so) ignoring LE for the soil. A new T_{so} and T_c values are found and sensible heat flux components are again estimated, and canopy LE computed. Then once again, the overall LE result is verified for a positive/negative sign.

Below is a list of equations used in the TSM application:

1. Fractional vegetation cover (fc), Norman et al. (1995):

$$fc = 1- EXP(-0.5*LAI) \quad \text{(A17)}$$

where LAI is leaf area index ($m^2\ m^{-2}$)

2. Local LAI (LAI_L), Kustas and Norman (2000):

$$LAI_L = LAI/fc \quad \text{(A18)}$$

3. Fractional soil cover (Fs), Kustas and Norman (2000):

$$Fs = [fc*(EXP(-0.5* LAI_L)]+(1-fc) \quad \text{(A19)}$$

4. Clumping factor (Ω), Kustas and Norman (2000):

$$\Omega = - LN(Fs)/(0.5*LAI) \quad \text{(A20)}$$

5. New (updated) fractional vegetation cover (fc_nw), Kustas and Norman (2000):

$$fc\_new = 1-EXP(-0.5* \Omega*LAI) \quad \text{(A21)}$$

6. Surface albedo (α), Brest and Goward (1987):

$$\alpha = 0.512*RED + 0.418*NIR \quad \text{(A22)}$$

where: RED and NIR are reflectance in the RED and NIR bands, respectively, obtained with the UAS.

7. Net radiation (Rn), Monteith (1973):

$$R_n = (1-\alpha)R_s + \varepsilon_a \sigma T_a^4 - \varepsilon_s \sigma T_s^4 \quad \text{(A23)}$$

a) Where the first term of Rn is the short wave radiation budget (Rsw):

$$Rsw = (1- \alpha)*Rs \quad \text{(A24)}$$

Where: Rs is the incoming short wave solar radiation, in W/m^2.

b) Calculate atmospheric/air long wave incoming radiation (Rlw_in):

$$\text{Rlw\_in} = \varepsilon_a \sigma T_a^4 \quad \text{(A25)}$$

Where σ is the Stefan-Boltzmann constant (5.67E-08 Watts m^{-2} K^{-4}), ε_a is emissivity and T_a temperature (K) from air.

c) Air emissivity (ε_a), Brutsaer (1975):

$$\varepsilon_a = 1.24\left(\frac{e_a}{T_a}\right)^{1/7} \quad \text{(A26)}$$

where, e_a is actual vapor pressure (mb) and T_a is air temperature (K) from weather station measurements.

d) Surface outgoing long wave radiation (Rlw_out):

$$\text{Rlw\_out} = \varepsilon_s \sigma\, T_s^4 \quad \text{(A27)}$$

Where subscript “s” denotes surface emissivity and temperature respectively.

e) Long wave radiation budget (Rlw):

$$Rlw = Rlw\_in – Rlw\_out \qquad (A28)$$

8. Extinction coefficient for canopy (K), Campbell (1986), Campbell and Norman (1998):

$$K = 1/(2*\cos(\theta_z*\pi/180)) \qquad (A29)$$

Where: θ_z is the solar zenith angle in degrees, and π is 3.1416.

9. The components of "Rs", i.e. the direct beam and the diffuse solar radiation parts. (Spokas and Forcella, 2006):

$$Rs = Rb + Rd \qquad (A30)$$

Where: Rb is direct beam and Rd the diffuse solar radiation.

a) The optical air mass number (m).

$$m = P/(101.3*\cos(\theta_z*\pi/180)) \qquad (A31)$$

Where: P is barometric pressure in kPa, from a weather station.

b) Rb as: $Rb = Gsc \times (\tau_{atm})^m$ (A32)

where Gsc is the solar constant (1360 W/m^2), and τ_{atm} is the atmospheric transmittance (which is calculated in MODTRAN) or transmissivity (ASCE EWRI, 2005).

c) Rd as: $Rd = 0.3*(1- (\tau_{atm})^m)*Gsc*\cos(\theta_z* \pi/180)$ (A33)

10. Fraction (fb) of incident PAR (photosynthetically active radiation) from Rb, Goudriaan (1977):

$$fb = Rb/(Rb+Rd) \qquad (A34)$$

11. Solar transmittance in the canopy (τ_c), Norman and Jarvis (1974):

$$\tau_c = EXP((a*(1-0.47*fb))*LAI)/(((1-(1/(2*K)))*fb)-1)) \qquad (A35)$$

12. Initial canopy net radiation (dRn), Norman et al. (1995):

$$dRn = Rn-(Rn*EXP(0.9*LN(1-fc\_nw))) \tag{A36}$$

13. Initial sensible heat flux for canopy (Hc_in), Priestly and Taylor (1972):

$$Hc\_in = dRn*(1-(1.3*fg*\Delta/(\Delta*\gamma))) \tag{A37}$$

Where: fg is fraction of the LAI that is green, Δ is the slope of the saturation vapor pressure versus temperature curve, and γ is the psychrometer constant.

14. Initial aerodynamic resistance to heat transfer (rah_in). Monin-Obukhov similarity theory (Foken, 2006), and (Liu et al. 2006). Below, the iteration utilized to correct H and rah for stability is depicted.

$$u_* = \frac{U \quad \kappa}{Ln\left(\frac{Z_m - d}{Z_{om}}\right)}$$

$$L_{M\_O} = \frac{-u_*^{\,3}\, T_a\, \rho_a\, C_{pa}}{g\, k\, H}$$

$$r_a = \frac{\ln\left[\frac{z-d}{z_{om}}\right]\ln\left[\frac{z-d}{z_{oh}}\right]}{uk^2}$$

$$Hc = \rho_a\, Cp_a\, (T_c - T_a) / r_{ah}$$

$$x = \left(1 - 16*\frac{Z_m - d}{L_{M\_O}}\right)^{\frac{1}{4}}$$

T_c

$$\psi_m = 2*Ln\left(\frac{1+x}{2}\right) + Ln\left(\frac{1+x^2}{2}\right) - 2*a\tan(x) + \frac{\pi}{2}$$

$$\psi_h = 2*Ln\left(\frac{1+x^2}{2}\right)$$

$$u_* = \frac{U \quad \kappa}{Ln\left(\frac{Z_m - d}{Z_{om}}\right) - \psi_m\left(\frac{Z_m - d}{L_{M\_O}}\right) + \psi_m\left(\frac{Z_{om}}{L_{M\_O}}\right)}$$

$$r_{ah} = \frac{Ln\left(\frac{Z_m - d}{Z_{oh}}\right) - \psi_h\left(\frac{Z_m - d}{L_{M\_O}}\right) + \psi_h\left(\frac{Z_{oh}}{L_{M\_O}}\right)}{u_* \quad \kappa}$$

If $r_{ah\_i-1} = r_{ah\_i}$

Where,

Tc is canopy temperature in K. Tc is initially estimated using Hc_in and rah estimated for neutral atmospheric conditions.

$$Tc\_in = ((Hc\_in * rah)/(\rho_a * Cp_a)) + Ta \tag{A38}$$

Where, ρ_a is air densigy, Cp_a specific heat of air, and Ta is air temperature.

Then, tto correct H for atmospheric stability conditions:

$$r_{ah} = \frac{\ln\left(\frac{Z_m - d}{Z_{oh}}\right) - \psi_h\left(\frac{Z_m - d}{L_{M\_O}}\right) + \psi_h\left(\frac{Z_{oh}}{L_{M\_O}}\right)}{u_* \quad k} \tag{A39}$$

where ψ_h is the stability correction factor for atmospheric heat transfer. L_{M_O} is Monin-Obukhov length scale, (m). u_* is friction velocity, (m s^{-1}).

According to Monteith and Unsworth (1990), L_{M_O} can be expressed as follows:

$$L_{M\_O} = \frac{-u_*^3\ T_a\ \rho_a\ C_{pa}}{g\ k\ H} \tag{A40}$$

where g is the earth gravity acceleration. The stability correction factor for atmospheric heat transfer ψ_h, for unstable conditions ($L_{M\_O} < 0$), is:

$$\psi_h = 2\ln\left(\frac{1 + x^2}{2}\right) \tag{A41}$$

$$x = \left(1 - 16\ \frac{Z_m - d}{L_{M\_O}}\right)^{\frac{1}{4}} \tag{A42}$$

The friction velocity under neutral conditions ($L_{M\_O} \sim \infty$), is:

$$u_* = \frac{U \quad k}{\ln\left(\frac{Z_m - d}{Z_{om}}\right)} \tag{A43}$$

Considering diabatic or non-neutral conditions the friction velocity is:

$$u_* = \frac{U \quad k}{\ln\left(\frac{Z_m - d}{Z_{om}}\right) - \psi_m\left(\frac{Z_m - d}{L_{M\_O}}\right) + \psi_m\left(\frac{Z_{om}}{L_{M\_O}}\right)} \tag{A44}$$

Where, ψ_m is the stability correction factor for momentum transfer. For unstable conditions it is:

$$\psi_m = 2\ln\left(\frac{1+x}{2}\right) + \ln\left(\frac{1+x^2}{2}\right) - 2\,\mathrm{atan}(x) + \frac{\pi}{2} \qquad \text{(A45)}$$

15. The initial soil temperature (Ts_in) is, Norman et al. (1995):

$$Ts\_in = ((((Tsfc-273.15)^4)-(fc\_nw*Tc\_in)^4)/(1-fc\_nw))^{(1/4)} \qquad \text{(A46)}$$

Where: Tsfc is the radiometric surface temperature (K), from the UAS thermal camera.

16. The initial long wave radiation emitted by the canopy (Lc).

$$Lc = (\varepsilon\_c * \sigma *(Tc\_in+273.15)^4) \qquad \text{(A47)}$$

Where, ε_c is canopy emissivity, which is set to 0.98 for a good green vegetation stand.

17. Calculate the initial long wave radiation emitted by the soil (Ls).

$$Ls = (\varepsilon\_s * \sigma *(Ts\_in+273.15)^4) \qquad \text{(A48)}$$

Where, ε_s is soil emissivity, which is set to 0.92 for bare soil with high reflective properties.

18. Soil albedo (α_S), Post el al. (2000):

$$\alpha_S = (0.785*NIR)-(0.745*BLUE)+(0.872*GREEN)+0.01 \qquad \text{(A49)}$$

where: BLUE and GREEN are reflectance in the blue and green bands.

Note: Our TETRACAM does not have a BLUE band and therefore a linear calibration was used based on the GREEN band reflectance values. The calibration was developed with surface reflectance data obtained on the ground by a handheld multispectral scanner (MSR5, Cropscan). The MSR5 sensor has similar bandwidths as the ones from the TETRACAM and to Landsat 5 TM.

19. Short wave radiation for soil (Sns), Kustas and Norman (2000):

$$Sns = \tau_c*(1- \alpha_S)*Rs \qquad \text{(A50)}$$

Where Rs is incoming short wave radiation, W m^{-2}

20. Long wave net radiation from canopy (Lnc), Kustas and Norman (2000):

$$Lnc = (1-EXP(-Kl*\Omega*LAI))*(Rlw\_in + Ls – 2 * Lc) \quad (A51)$$

Where: Kl is an extinction coefficient set to 0.95.

21. Long wave net radiation from soil (Lns), Kustas and Norman (2000):

$$Lns = ((EXP(-Kl* \Omega *LAI))*Rlw\_in)+((1-EXP(-Kl* \Omega *LAI))*Lc)-Ls \quad (A52)$$

22. Net radiation for soil (Rns), Norman et al. (1995):

$$Rns = (Sns + Lns) \quad (A53)$$

23. Net radiation for canopy, Norman et al. (1995):

$$Rnc =(Rn - Rns) \quad (A54)$$

24. Sensible heat flux for canopy (Hc), Norman et al. (1995):

$$Hc = (Rnc*(1-(1.3*fg*(\Delta/(\Delta+\gamma))))) \quad (A55)$$

25. Using Hc from previous step rah is updated, to “rah_new,” using the Monin-Obukhov iterative procedure outlined previously.

26. Mean canopy leaf width (wc). For sorghum/corn it was assumed 0.09 m.

27. Extinction coefficient for wind function (a_ext), Norman et al. (1995):

$$a\_ext = 0.28*((\Omega*LAI)\text{^}(2/3))*(hcc\text{^}(1/3))*(wc\text{^}(-1/3)) \quad (A56)$$

where: hcc is crop height, m.

28. Wind speed at the top of the canopy (Uc), Norman et al. (1995):

$$Uc = =u*(LN((hcc-d)/Zmo)/(LN((Zm-d)/Zmo)- \psi_m)) \quad (A57)$$

Where: u is horizontal wind speed from weather station, m/s. d is the zero plane displacement. Zmo is the roughness length for momentum transfer, and ψ_m (m) is the stability correction factor for momentum transfer.

29. Wind speed close to the soil level (Us), Norman et al. (1995):

Us = =Uc*EXP(-a_ext*(1-(0.15/hcc))) (A58)

30. Resistance to heat flow just above the soil (rso), Norman et al. (1995):

rso = (1/(0.004+(0.012*Us))) (A59)

31. Total net radiation (Rn).

Rn = Rsw + Rlw (A60)

32. Soil heat flux (G), Chavez et al. (2005) or other proven equation:

G = (((0.3324+(-0.024*LAI))*(0.8155+(-0.3032*LN(LAI))))*Rn) (A61)

33. Updated canopy temperature (Tc).

Tc = ((Hc*rah_new)/(Rho*Cp))+Ta (A62)

34. Estimating an updated soil temperature (Tso), Norman et al. (1995):

Tso = (((Tsfc-273.15)^4 - (fc_nw*Tc)^4)/(1-fc_nw))^(1/4) (A63)

35. Compute sensible heat flux from soil (Hs), Norman et al. (1995):

Hs = =ρ_a*Cp_a*(Tso-Ta)/(rah_new+rso) (A64)

36. Compute total sensible heat flux (H): H = Hc + Hs (A65)

37. Estimate latent heat flux for the soil (LEs): LEs = Rns – Hs – G (A66)

38. Verification that Tso and Tc are correct, Norman et al. (1995):

If LEs >= 0 then correct and we have found a solution. If LEs < 0 then it is a dry soil, set LEs = 0 and make:

$$Hs = Rns - G \tag{A67}$$

Then recomputed Tso and Tc.

39. Total latent heat flux (LE, W/m^2).

$$LE = Rn - H - G \tag{A68}$$

Reflectance-based crop coefficient (Kc-NDVI)

The methodology presented in Neale et al. (1989) was adopted. In this approach, the normalized difference vegetation index (NDVI) is use to infer on the reflectance-based basal (transpiration) crop coefficient (Kcb). The NDVI obtained over a crop growing season was transformed into a reflectance based Kcb (K_{cr_NDVI}). Linearly NDVI of bare soil was related to Kcb of bare dry soil; while the NDVI at (crop) effective cover was related to Kcb at the same crop growth stage.

The equation shown below depicts the developed relationship for corn near Greeley, CO.

$$K_{cr\_NDVI} = 1.181 \times NDVI - 0.026 \tag{A69}$$

Where NDVI is:

$$NDVI = (R_{NIR} - R_{RED}) / (R_{NIR} + R_{RED}) \tag{A70}$$

Where R_{NIR} is surface reflectance (from UAS) in the NIR band and for the Red band is R_{RED}.

Once NDVI and K_{cr_NDVI} have been computed, daily actual crop water use is calculated by multiplying K_{cr_NDVI} by the alfalfa reference crop coefficient (ET_r).

$$ET = K_{cr\_NDVI} \times ET_r \tag{A71}$$

Reflectance-based crop coefficient (Kc-fc)

A similar approach, than the previous one, was developed by Trout and Johnson (2007) and by Johnson and Trout (2012). However, instead of using directly NDVI to update the crop coefficient, NDVI is converted to a vegetation fractional cover (fc) and then this "fc" in turn is converted to the reflectance based crop coefficient (K_{cr}) and then to crop actual transpiration, as illustrated below.

$NDVI \rightarrow f_c \rightarrow K_{cr} \rightarrow ET_a$

$$f_c = 1.22 \times NDVI - 0.21 \quad \text{(A72)}$$

$$K_{cr} = 1.13 \times f_c + 0.14 \quad \text{(A73)}$$

$$ET_a = K_{cr} \times ET_{ref} \quad \text{(A74)}$$

Where ET_{ref} is the reference ET calculated following the procedure outlined in ASCE-EWRI (2005).

APPENDIX B

ET MAPS

ARDEC CIG 1070: 22JUL15 K_cr

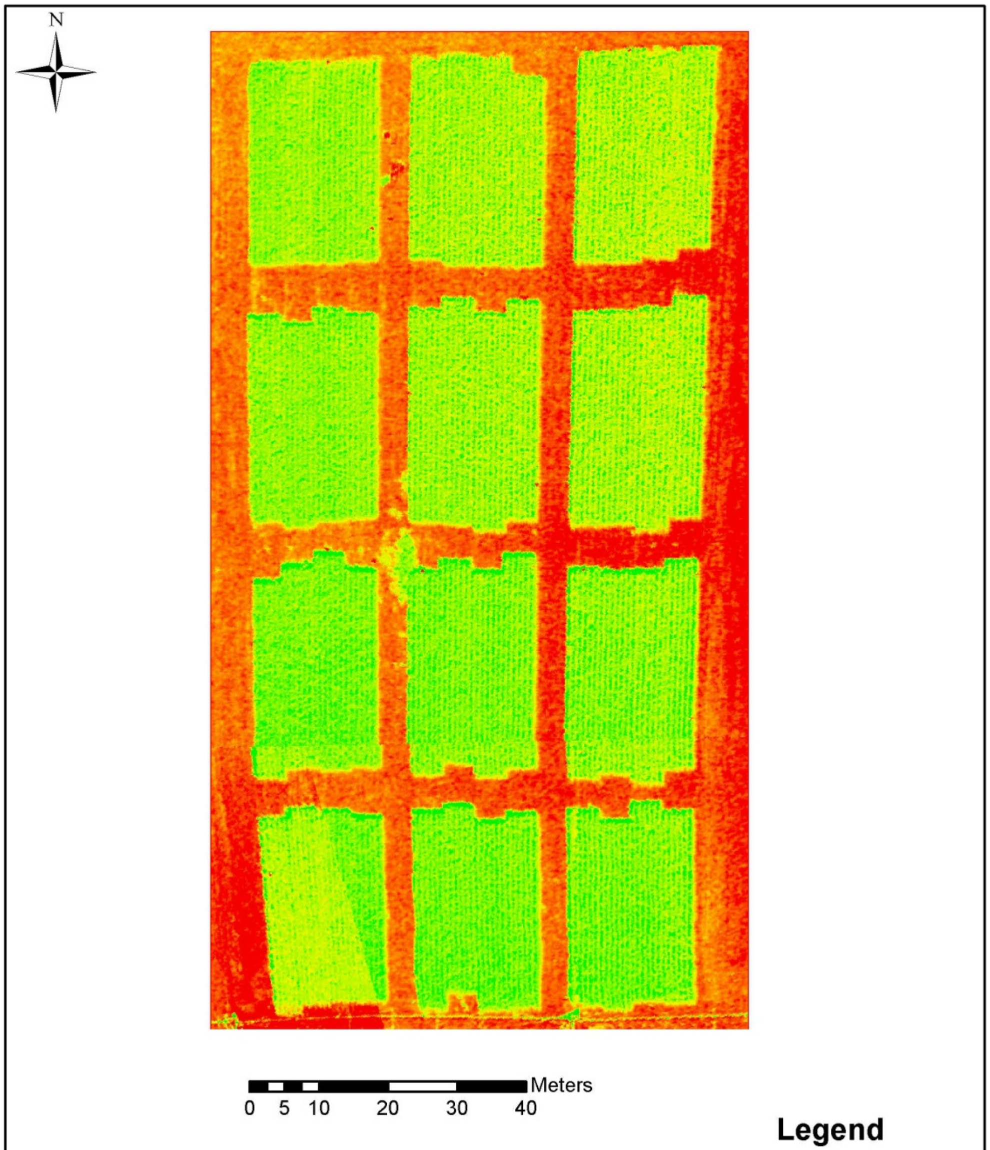

Date: 22JUL15
Location: CSU ARDEC CIG 1070
Aircraft: CSU Tempest
Collection: NIR, Red, Green, Thermal, Digital Imagery
Overpass Time: 1115 MDT (+6 GMT)
Altitude: 400 ft AGL
Resolution: 12 cm
Method: K_cr

ARDEC CIG 1070: 13AUG15 K_cr

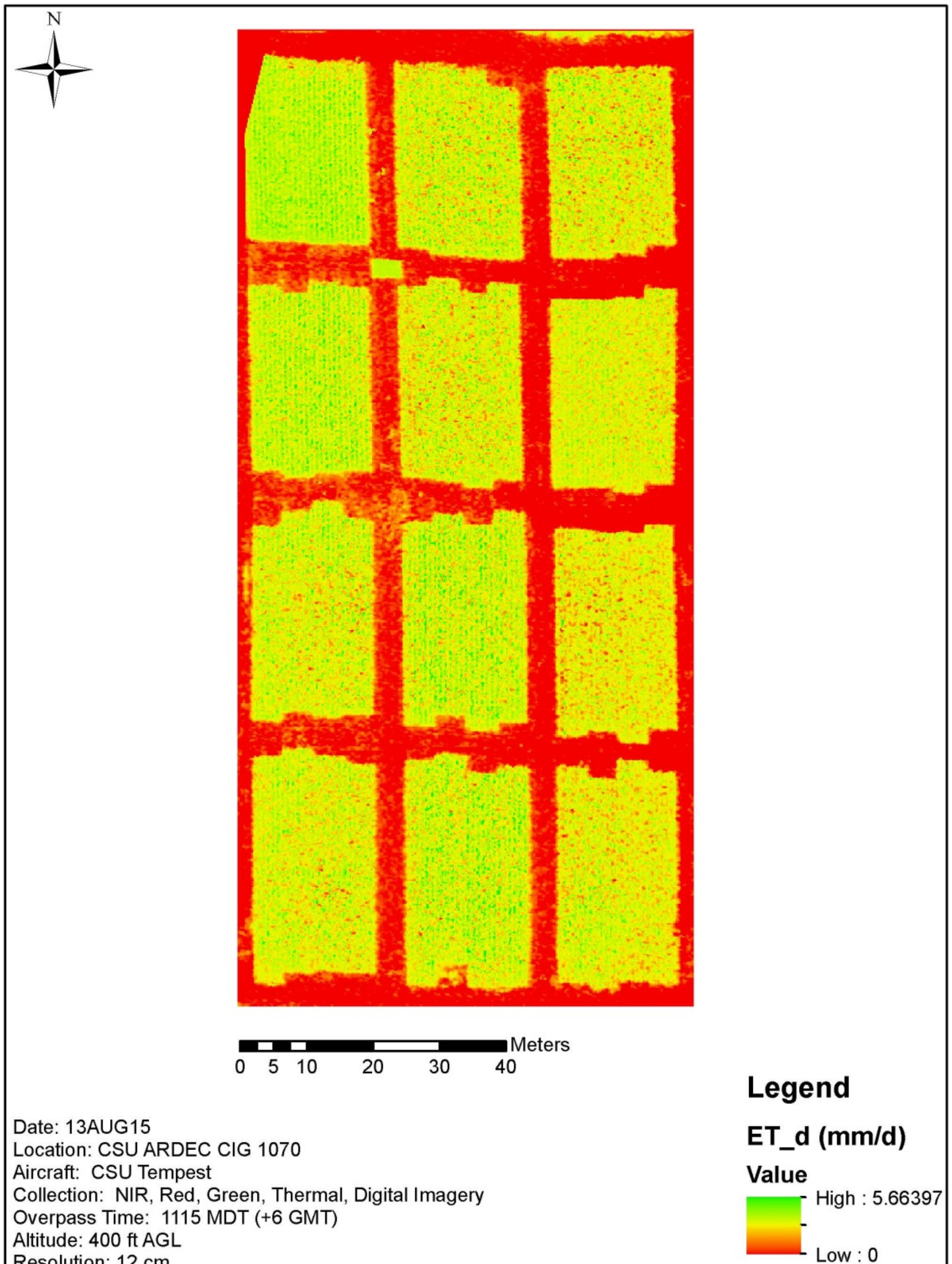

Date: 13AUG15
Location: CSU ARDEC CIG 1070
Aircraft: CSU Tempest
Collection: NIR, Red, Green, Thermal, Digital Imagery
Overpass Time: 1115 MDT (+6 GMT)
Altitude: 400 ft AGL
Resolution: 12 cm
Method: K_cr

ARDEC CIG 1070: 10SEP15 K_cr

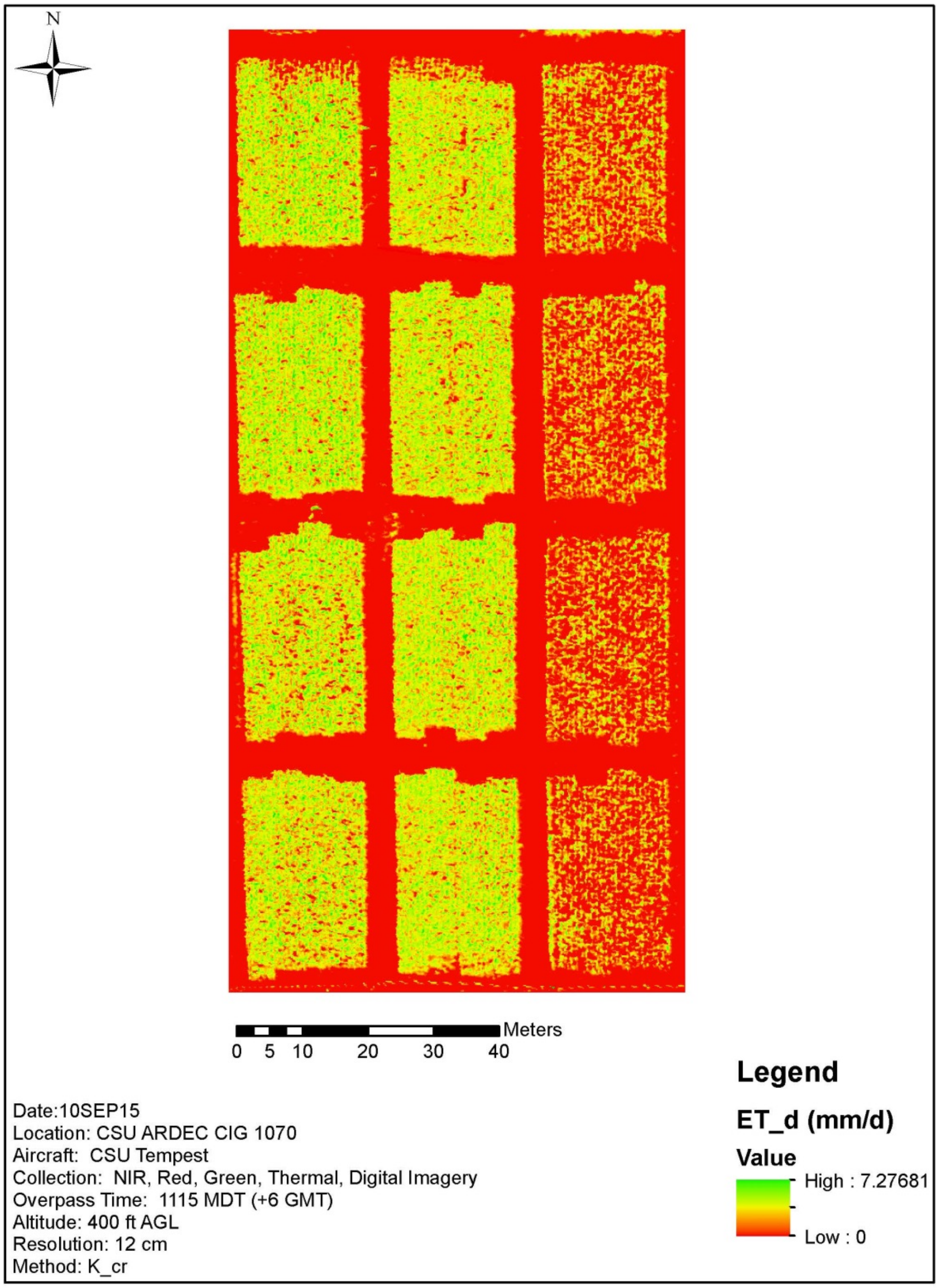

Date:10SEP15
Location: CSU ARDEC CIG 1070
Aircraft: CSU Tempest
Collection: NIR, Red, Green, Thermal, Digital Imagery
Overpass Time: 1115 MDT (+6 GMT)
Altitude: 400 ft AGL
Resolution: 12 cm
Method: K_cr

ARDEC CIG 1070: 13AUG15 CWSI

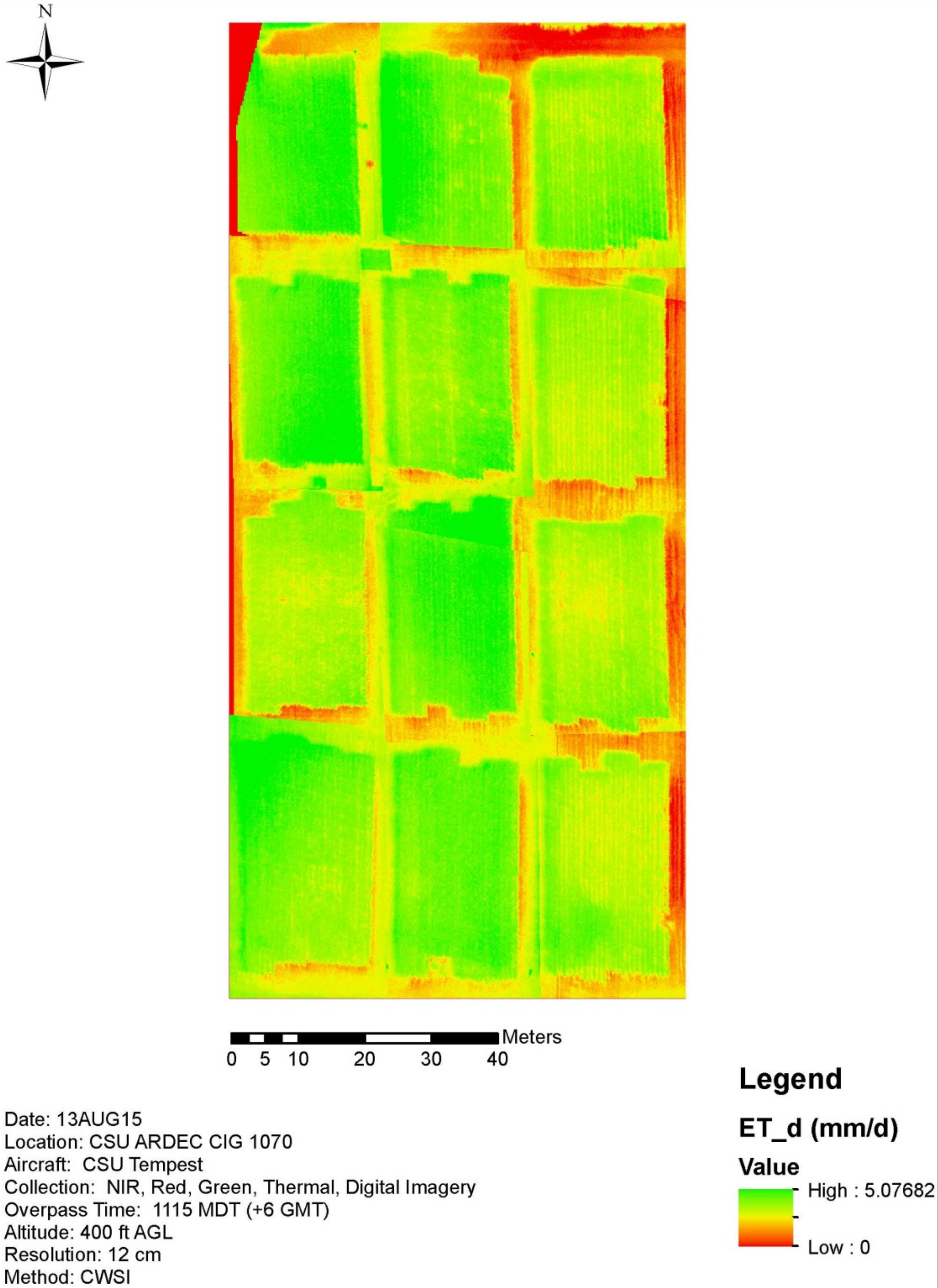

Date: 13AUG15
Location: CSU ARDEC CIG 1070
Aircraft: CSU Tempest
Collection: NIR, Red, Green, Thermal, Digital Imagery
Overpass Time: 1115 MDT (+6 GMT)
Altitude: 400 ft AGL
Resolution: 12 cm
Method: CWSI

ARDEC CIG 1070: 10SEP15 CWSI

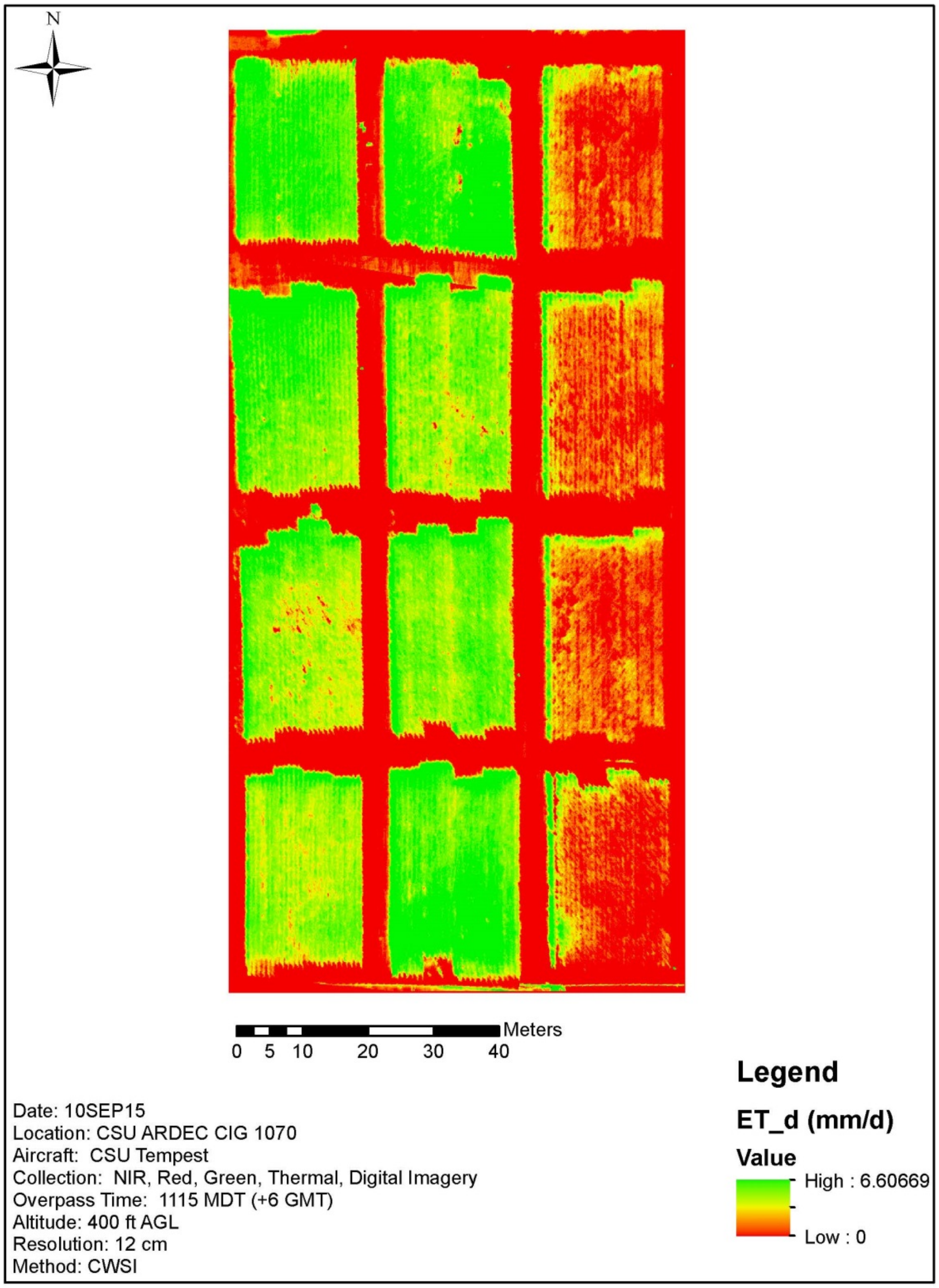

ARDEC CIG 1070: 13AUG15 TSEB

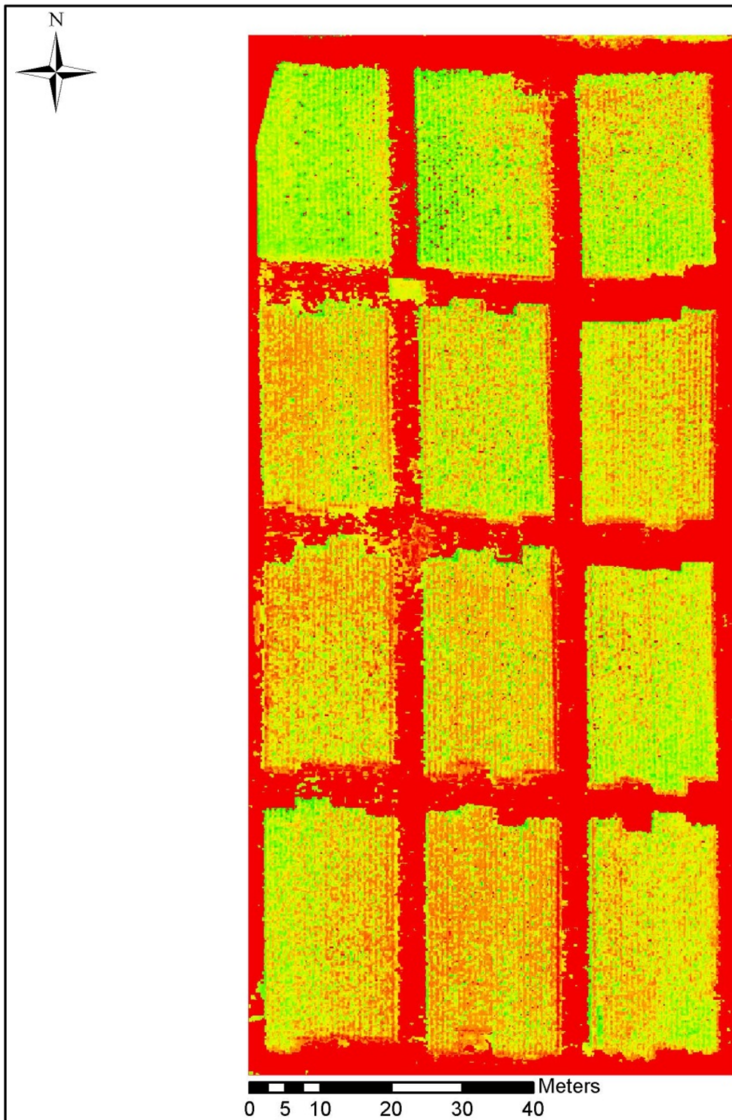

Legend

ET_d (mm/d)

Value

High : 3.5

Low : 0

Date: 13AUG15
Location: CSU ARDEC CIG 1070
Aircraft: CSU Tempest
Collection: NIR, Red, Green, Thermal, Digital Imagery
Overpass Time: 1115 MDT (+6 GMT)
Altitude: 400 ft AGL
Resolution: 12 cm
Method: Two Source Energy Balance

ARDEC CIG 1070: 10SEP15 TSEB

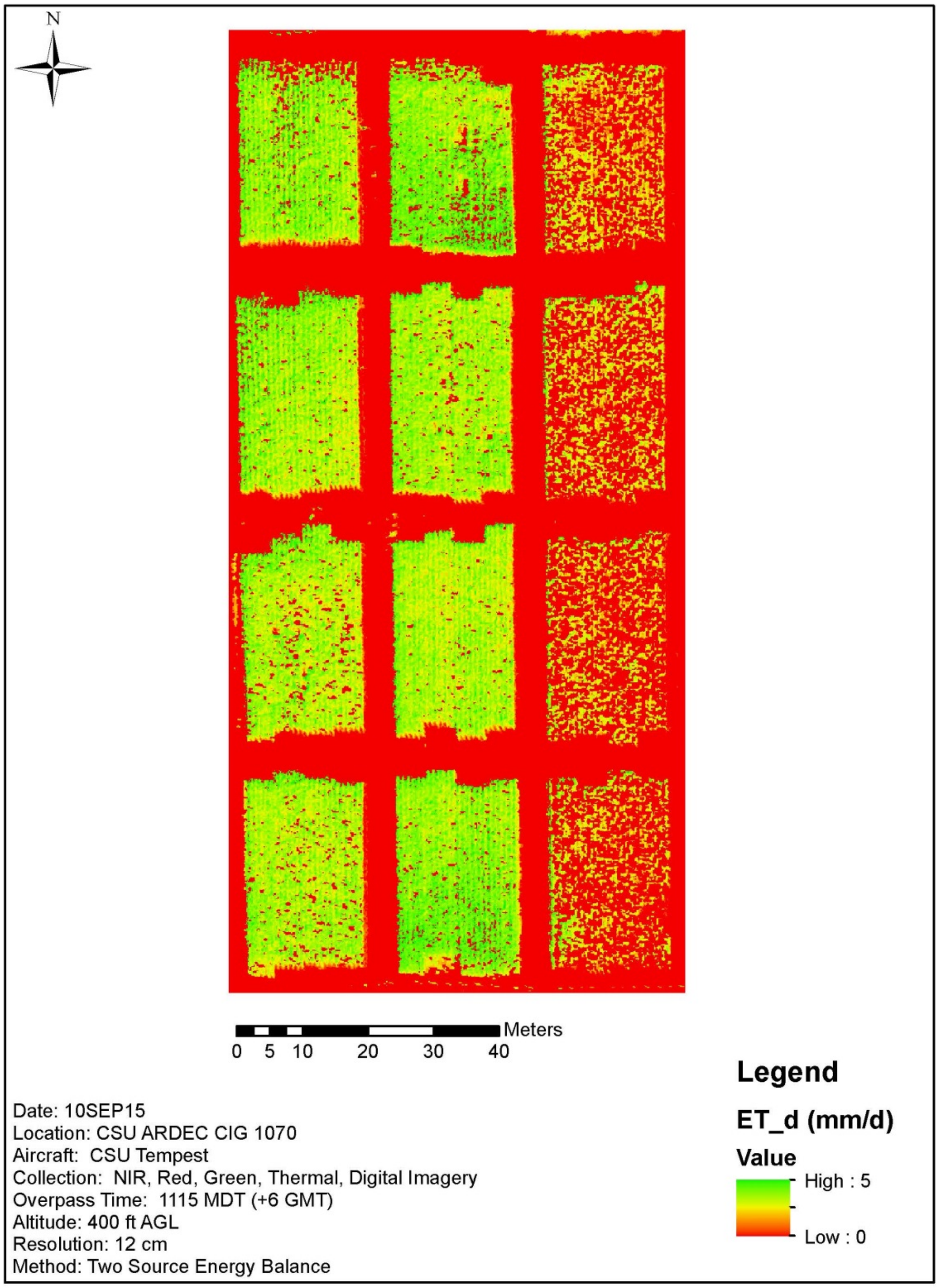

ARDEC CIG: 13AUG15 SAT

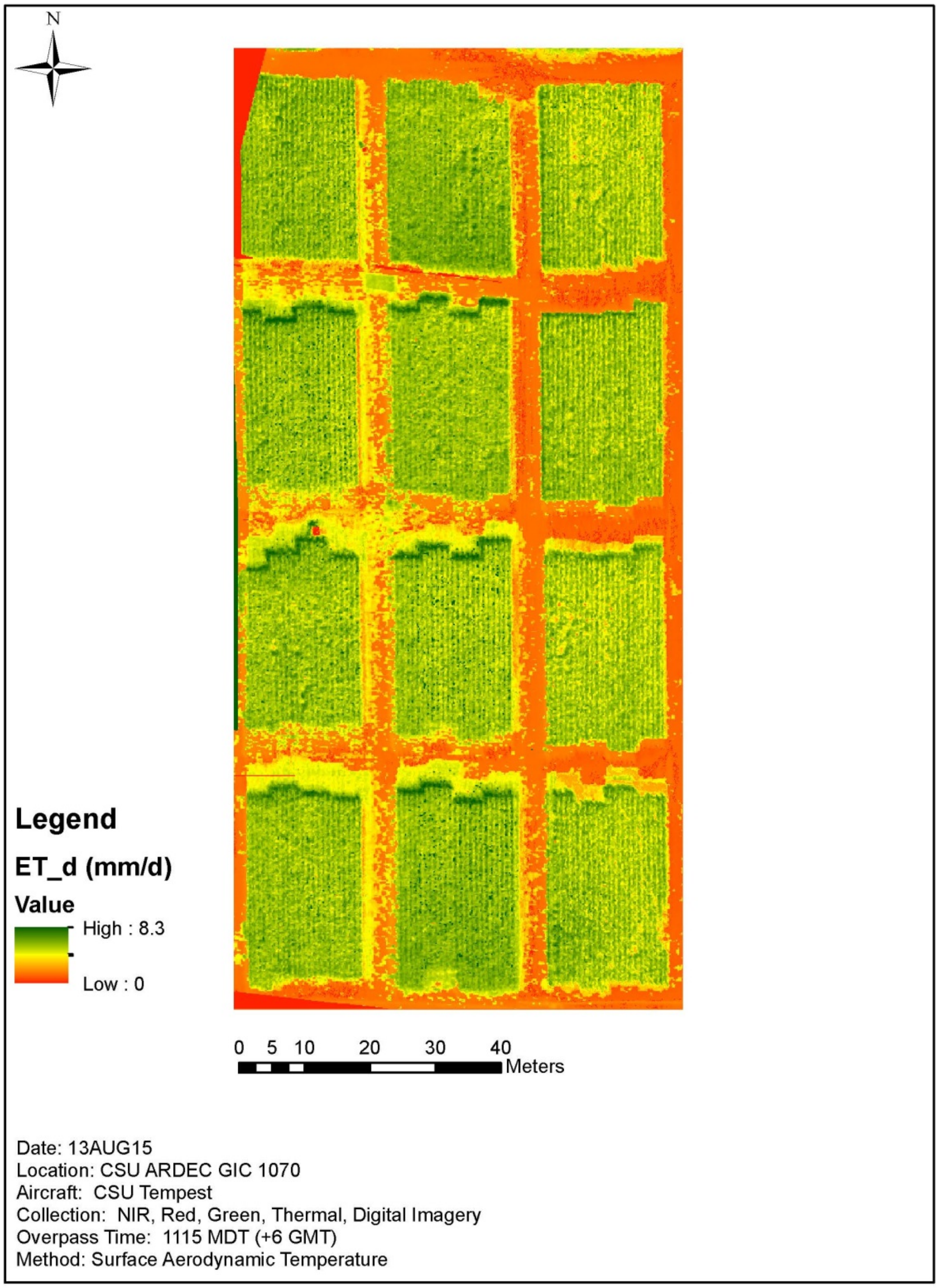

ARDEC CIG 1070: 10SEP15 SAT

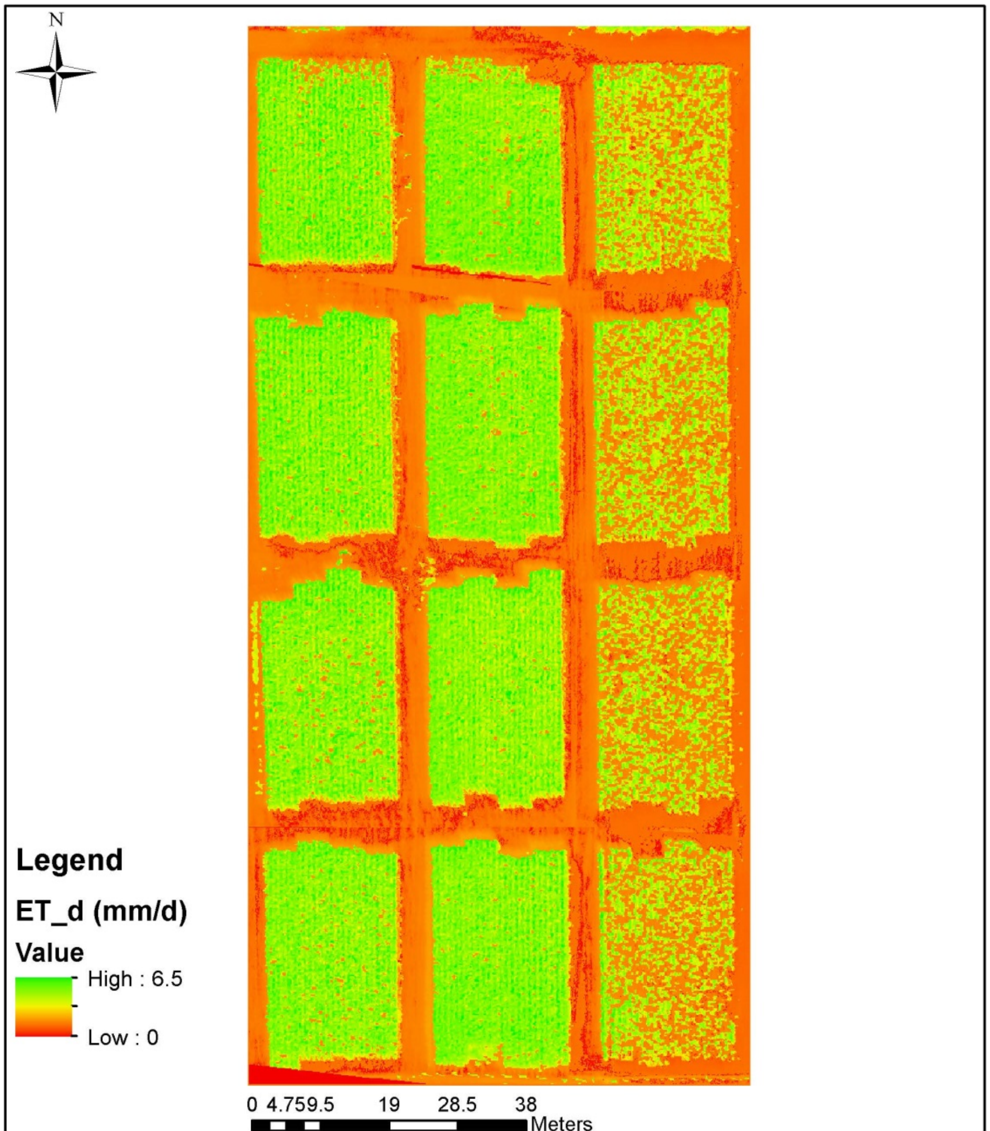

Date: 10SEP15
Location: CSU ARDEC GIC 1070
Aircraft: CSU Tempest
Collection: NIR, Red, Green, Thermal, Digital Imagery
Overpass Time: 1115 MDT (+6 GMT)
Method: Surface Aerodynamic Temperature

CSU AVRC: Sorghum 18SEP15 K_cr

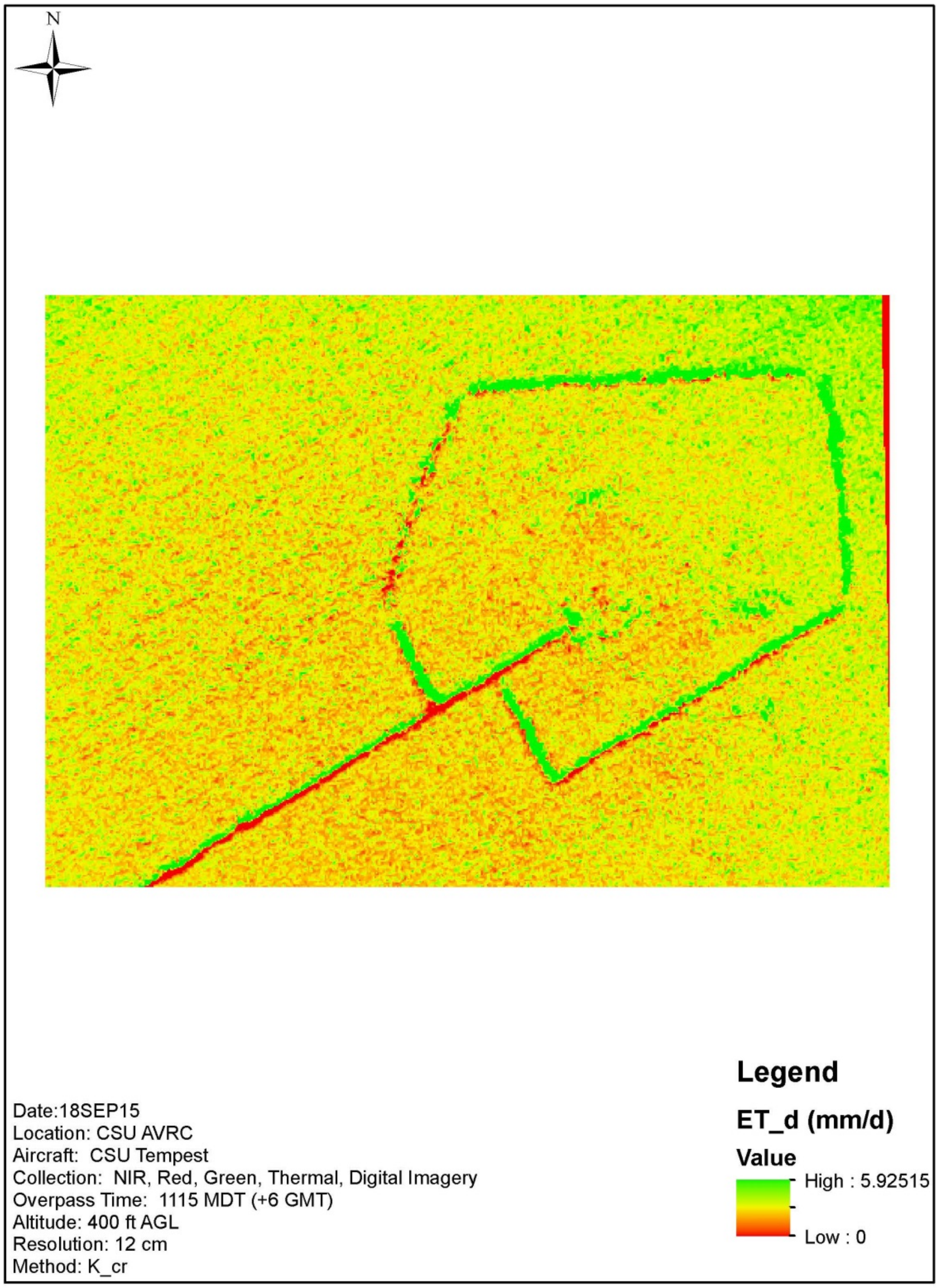

CSU AVRC: Sorghum 18SEP15

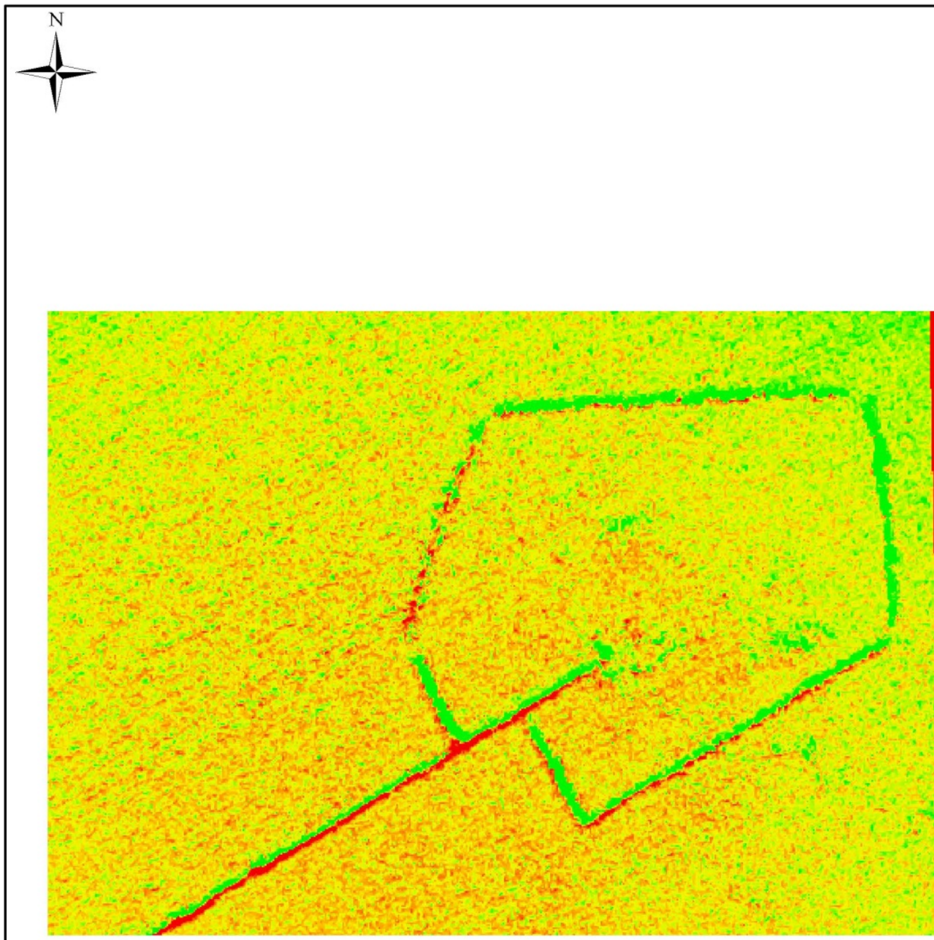

Date:18SEP15
Location: CSU AVRC
Aircraft: CSU Tempest
Collection: NIR, Red, Green, Thermal, Digital Imagery
Overpass Time: 1115 MDT (+6 GMT)
Altitude: 400 ft AGL
Resolution: 12 cm
Method: SAT

Legend

ET_d (mm/d)

Value

High : 5.92515

Low : 0

CSU AVRC: Sorghum 18SEP15 TSEB

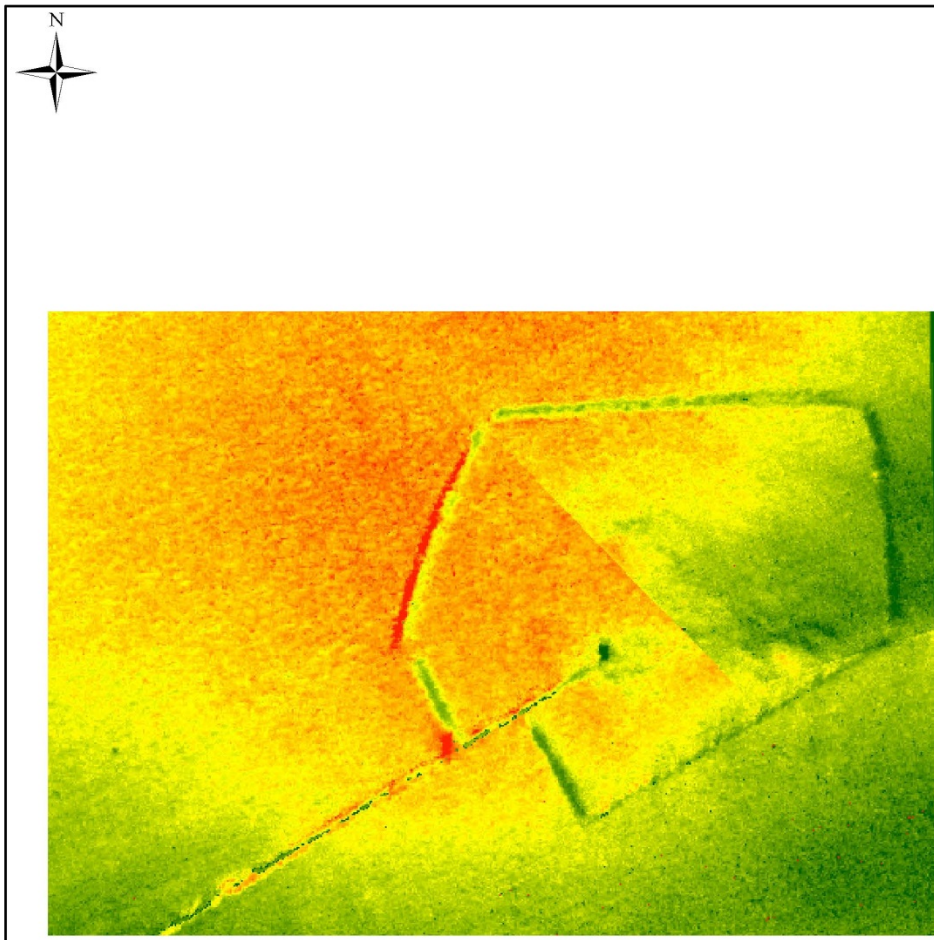

Date:18SEP15
Location: CSU AVRC
Aircraft: CSU Tempest
Collection: NIR, Red, Green, Thermal, Digital Imagery
Overpass Time: 1115 MDT (+6 GMT)
Altitude: 400 ft AGL
Resolution: 12 cm
Method: TSEB

Legend

ET_d (mm/d)

Value

High : 7.35

Low : 0

Northern Water: 23SEP15 K_cr

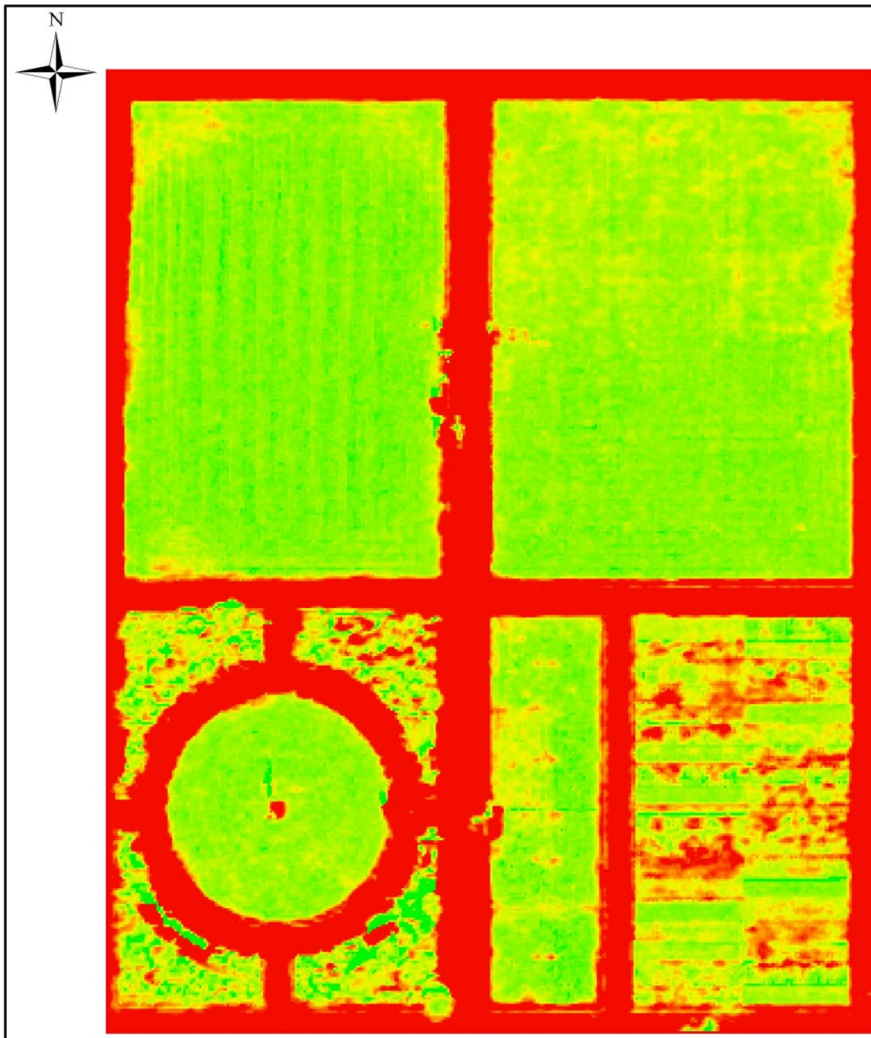

Date:23SEP15
Location: Northern Water
Aircraft: CSU Tempest
Collection: NIR, Red, Green, Thermal, Digital Imagery
Overpass Time: 1115 MDT (+6 GMT)
Altitude: 400 ft AGL
Resolution: 12 cm
Method: K_cr

Legend

ET_d (mm/d)

Value

High : 4.9147

Low : 0

Northern Water: 23SEP15 SAT

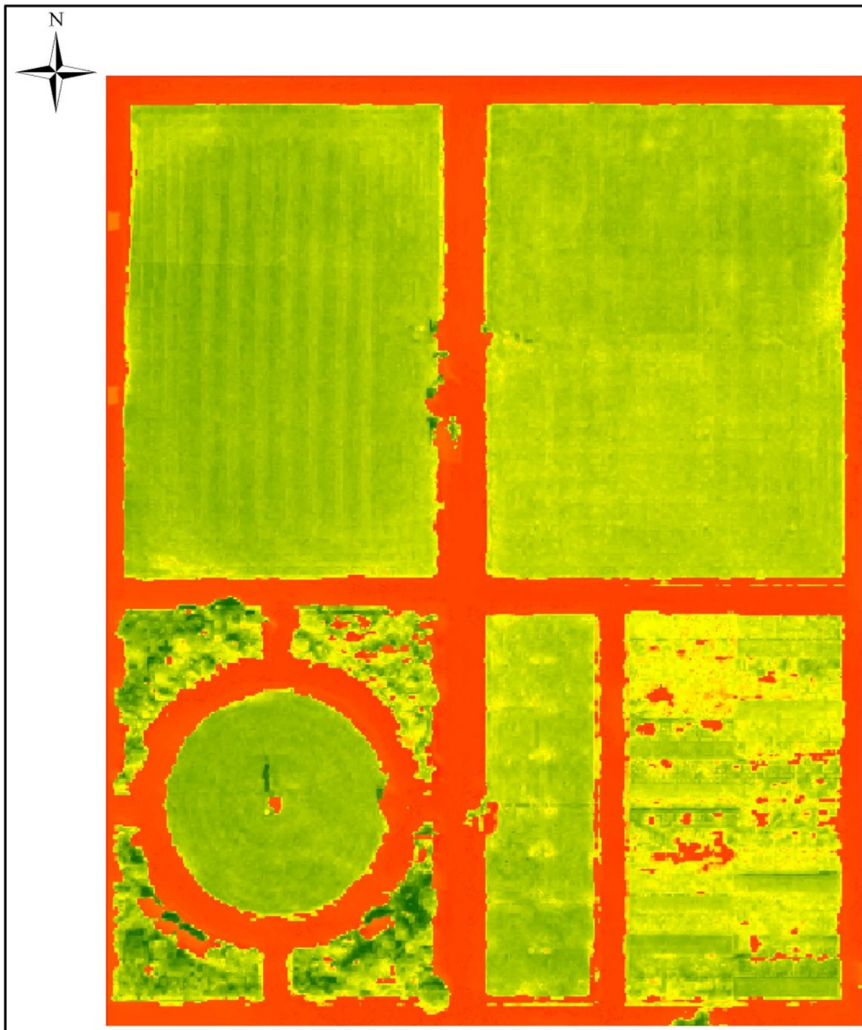

Legend

ET_d (mm/d)

Value

High : 5.46182

Low : 0

Date: 23SEP15
Location: Northern Water
Aircraft: CSU Tempest
Collection: NIR, Red, Green, Thermal, Digital Imagery
Overpass Time: 1115 MDT (+6 GMT)
Altitude: 400 ft AGL
Resolution: 12 cm
Method: Surface Aerodynamic Temperature

Northern Water: 23SEP15 TSEB

Date:23SEP15
Location: Northern Water
Aircraft: CSU Tempest
Collection: NIR, Red, Green, Thermal, Digital Imagery
Overpass Time: 1115 MDT (+6 GMT)
Altitude: 400 ft AGL
Resolution: 12 cm
Method: TSEB

Legend

ET_d (mm/d)

Value

High : 3.65

Low : 0